 DOI 10.1515/pac-2013-1021 — Pure Appl. Chem. 2014; 86(5): 611–632

Conference paper

Deepak P. Dubal and Rudolf Holze*

Synthesis, properties, and performance of nanostructured metal oxides for supercapacitors

Abstract: Beyond activated carbon and other forms of high-surface area carbon operating solely as double layer storage materials in capacitors of high capacitance commonly somewhat imprecisely called supercapacitors other electrode materials storing electric charge by reversible and fast superficial redox processes are studied as active masses. The resulting devices combining double layer and Faradaic process-based charge storage – commonly called hybrid ones – show significantly higher capacitances at only marginally diminished power capability. Among the suggested materials metal oxides feature most prominently. Their formation, characterization and properties together with the performance of prepared devices are reviewed here.

Keywords: double layer; electrochemistry; electrodes; energy conversion; metal oxides; NMS-IX; pseudocapacitance; supercapacitors.

***Corresponding author: Rudolf Holze,** Technische Universität Chemnitz, Institut für Chemie, AG Elektrochemie, D-09107 Chemnitz, Germany, e-mail: dubaldeepak2@gmail.com
Deepak P. Dubal: Technische Universität Chemnitz, Institut für Chemie, AG Elektrochemie, D-09107 Chemnitz, Germany

Article note: A collection of invited papers based on presentations at the 9th International Conference on Novel Materials and their Synthesis (NMS-IX), Shanghai, China, 17–22 October 2013.

The basics

Electric energy cannot be stored directly in amounts large enough to gain commercial viability. Systems employing e.g., superconductors or dielectric capacitors are either too large or too expensive in order to be of any wide importance (for examples and a brief review see [1]). Thus, basically two modes of rather direct storage employing chemical, more specifically physico-chemical, and electrochemical principles remain: Storage based on charge separation in the electrochemical double layer (i.e., capacitors) or storage based on the reversible conversion of electrical into chemical energy and vice versa $A + B \leftrightarrows C + D$: the accumulator (see Fig. 1).

For various reasons the former mode has for a long time been associated with high power mostly because of the inherently fast processes leaving out any interfacial electrochemical reaction limited by the inherent constraints of interfacial processes and the latter with high energy because of the much larger amounts of energy which could be stored based on associated chemical conversion reactions. This is also the inherent reason of the lower power of the latter devices, interfacial reactions mostly associated with phase transformations and extended transport of matter tend to be slow. The energy density of the former devices tends to be low because of the limited amount of interfacial surface area available in any given device. This is illustrated in a Ragone plot showing some examples of storage devices (see Fig. 2).

As indicated devices based on traditional electrolytic capacitor technologies (as in aluminum foil- or tantalum-pentoxide-based ones) show highest power density. Although these devices are based only on the movement and separation of electric charges without any chemical reaction being involved a short characterization of salient features may be helpful to settle the current confusion about these various devices.

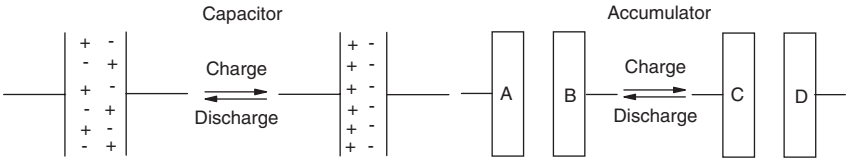

Fig. 1 Distinguishing a capacitor from an accumulator.

Basically a capacitor is simply composed of two electronically conducting plates of e.g., metal separated by an insulating (dielectric) material (see Fig. 1). The capacitance C defined as

$$C = \frac{Q}{U} \tag{1}$$

with the stored charge Q at a voltage U of this two-plate condenser is given by the surface area of the two plates, their distance and the properties of the matter in between according to

$$C = \frac{\varepsilon_r \varepsilon_0}{d} A \tag{2}$$

with ε_r = relative electrolyte dielectric constant, ε_0 = dielectric constant of the vacuum, d = distance between the plates and A = surface area of the plates. In an electrolytic capacitor the distance shrinks to the thickness of the insulating aluminum or tantalum oxide whereas the surface area may reach large values because of the highly porous surface area of the participating electron-conducting electrodes. Actually already this electroyltic capacitor is composed of two capacitances connected in series: The capacitance C_{diel} already described given by the metal foil or porous body with the thin film of metal oxide on it as the dielectric and the liquid or gelled electrolyte solution soaked into the separator acting as the "counterelectrode." The second aluminum foil (in case of tantalum condensers it may also be a porous layer of carbon powder) is in contact with this electrolyte, thus an electrochemical double layer is established. Its capacitance C_{dl} is so large that the actual and resulting value of the series connection is controlled by the smaller capacitance of the former contribution (see Fig. 3).

Thus the resulting capacitance C is given by

$$\frac{1}{C} = \frac{1}{C_{\text{diel}}} + \frac{1}{C_{\text{dl}}} \approx \frac{1}{C_{\text{diel}}} \tag{3}$$

The basically huge double layer capacitance can be employed even more effectively by putting two electrodes in contact with an electrolyte solution between them. Now two electrochemical double layers are "connected in series."

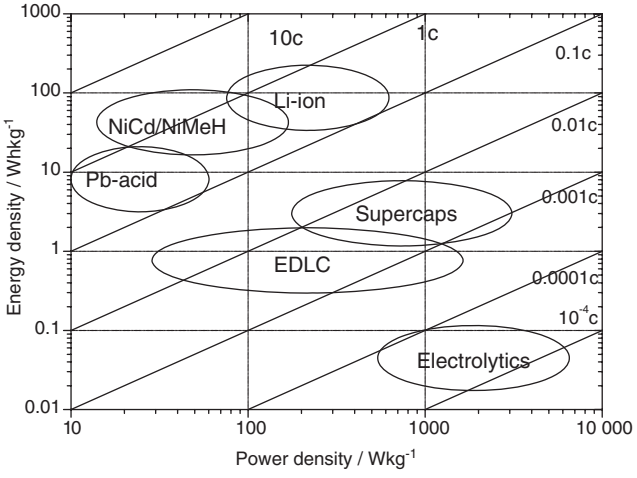

Fig. 2 Ragone plot for selected electrochemical storage and conversion systems [1].

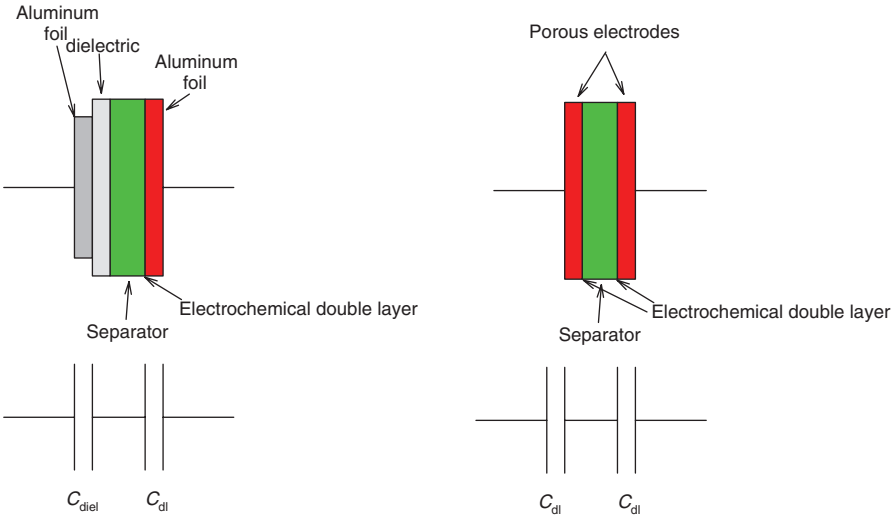

Fig. 3 Schematic of an electrolytic capacitor (top left) and its equivalent circuit (bottom left) and of a double layer capacitor (top right) and its equivalent circuit (bottom right).

The actual capacitance depends on the surface areas of both electrodes and the dielectric properties of the electrolyte solution, in particular the solvent. The previous scheme is modified as shown above. Devices thus employing only double layer charging (in EDLC) show already substantially higher energy density than electrolytic capacitors, easily several Farad as compared to micro- or milli-Farad – albeit at a limited power density because of the lower operating voltage. Different from the electrolytic capacitor, where the voltage drop is found across the highly insulating dielectric with the voltage drop across the double layer also present being of only minor importance the EDLC is basically an electrochemical cell with the electric energy stored as spacially separated charges. Given a sufficiently large voltage applied to the cell the electrolyte solution inside it will be electrolyzed, i.e., decomposed. In case of water the thermodynamic value amounts to $U = 1.229$ V [2], and even though this completely undesirable process depends not only on thermodynamics (i.e., energetics) but also on kinetics the rather low voltages possible under practical conditions cause a serious limitation even when species are added to the electrode materials somewhat impeding anodic and cathodic reactions. This can be overcome to some extent by using nonaqueous solvents with substantially larger decomposition voltages or with ionic liquids composed entirely of ions (i.e., molten salts with melting points around room temperature). Unfortunately these solvents and solution yield lower conductance values (for an overview see [3], for a thorough discussion and a listing of values see [4]). The claim, that aqueous solutions can be prepared and utilized without stringent control is erroneous [5], traces of dioxygen have frequently resulted in decreased capacitance values, losses and severe corrosion (for examples see below). This lower conductance in turn increases the electrical or equivalent series resistance ESR[1] of the capacitor, i.e., the sum of the Ohmic components of the capacitors impedance due to limited electronic conductance of the active masses, the wire leads, the current collector and mostly the ionic conductance of the electrolytic medium between the active masses. Low ESR values are of outmost importance in applications with voltage fluctuations of high frequency as e.g., in switching power supplies and voltage converters. Nevertheless capacitors of the EDLC-type have gained significant market share in particular for applications with low operating voltage and small power demand like for memory devices (SRAMs) (for an overview see e.g., [6–8]). Given the somewhat fuzzy history of the term supercapacitor[2] these devices have apparently been the first ones (A bibliometric study implies, that supercapacitor is the most popular term so far [9]). As compared

1 The symbol R_s should not be used instead of ESR [5] because it will be confused with the generally accepted use of R_s for serial resistance component in impedance data display and handling as well as with the solution R_s in electrochemistry.

2 The terms supercap or supercapacitor™ (as well as ultracap/ultracapacitor) appear to lack a proper and generally accepted definition. At first glance it appears sufficient to assume, that capacitors based on the capacitive properties of the electrochemi-

to electrolytic capacitors they are getting closer to the energy density of accumulators at improved power densities (for a detailed discussion of the underlying phenomena see e.g., [10–12]). In case of an EDLC the surface area may be much larger than in an electrolytic capacitor because of the large surface areas of the most frequently employed carbon-based materials (easily more than 2000 m^2 per gram of carbon material, for a thorough discussion see e.g., [13], this concept was discovered more coincidentally during research on high-surface area for fuel cells and subsequently patented [14], because of the impracticality of this approach employing flooded electrodes later patents starting with Rightmire's [15] may be considered as a more appropriate starting point) and because there is no dielectric insulating material of a certain thickness like said metal oxides in the electrolytic capacitor as discussed above. Instead the charges – actually ions on the electrolyte solution side and the electrons in the carbon (represented frequently in the jellium model [16]) – are only separated by the metal/solution interface. Nevertheless actually obtained capacities are lower than expected from surface area data as determined for carbon-based materials using e.g., the BET-method. Instead data follow the experimentally determined pore volume for at least a selection of carbons [17]. This has been ascribed to space constraints for accommodation of charged species (for a discussion see e.g., [18]). This comes as no surprise: Ever larger surface areas come associated with ever smaller pores only, and for charge storage ions have to move into these pores to the electrochemical interface located there. Below a critical pore size this is simply impossible, the actual value of this pore size depends on the ion size, degree of solvation, size of solvation shell etc.

Further increased capacities have become available only by going beyond charge storage in the double layer and by utilizing Faradaic processes in surface and subsurface layers of the electrochemically active electrode materials. These processes show up frequently in cyclic voltamograms CVs with an almost capacitor-like response as illustrated following with a CV (see Fig. 4).

The displayed selection (right) shows only weak waves superimposed on a rather constant current when changing the potential into the positive going (top) as well as the negative going (bottom) direction. The complete CV (left) shows further processes with well pronounced peaks, in particular of the reduction of the previously formed surface oxides proceeding in two stages because of shifting pH-values at the interface in the presence of an unbuffered, almost neutral electrolyte solution. Because the appearance of the current–potential relationship closely resemble that of a simple capacitor (for further examples see e.g., [19]) the current as well as the underlying phenomena have been called "pseudocapacitive" (for a thorough discussion see [20]). In the present case – with gold being fundamentally similar in behavior to ruthenium – the Faradic process involves surface redox processes associated here with the formation of gold hydroxide, oxide and its hydrous forms [21], consequently it has been called a *redox pseudocapacitance* (this term being attributed to Conway and Gileadi [22]). The capacitive-like behavior is initially due to the surface confinement of the redox reaction with the amount of converted species closely tracking surface coverage, current and electrode potential. Similar observations have been made with e.g., intrinsically conducting polymers ICPs [23] although the mechanism is completely different. With ICPs the wide distribution of actual length of oligo- and polymers, more precisely the length of conjugated segments (not to be confused with the effective conjugation length) varies widely, and accordingly oxidation (and subsequently reduction) potentials vary providing an almost continuum of redox peaks merged into the observed flat

cal double layer instead of a dielectric material like Al_2O_3 or Ta_2O_5 showing huge capacities are correctly called supercapacitors. Temporarily the latter term was trademarked (from August 1978 on) to NEC Corporation, currently this protection has apparently expired. The acronym SC seems to be too short to enable immediate identification. Acronyms like ES for electrochemical supercapacitor or FS for Faradaic supercapacitor do nothing beyond enlarging the confusion. Recently this device wherein purely electrostatic charge storage in the double layer is operative has been frequently called EDLC (electrochemical double layer capacitor). Thus it appears to be reasonable to call devices, wherein charge storage is based both on electrostatic charge separation (like in an EDLC) and on Faradaic redox processes (pseudocapacity) supercapacitors. Because of the combination of these fundamentally different charge storage mechanisms these devices are also sometimes called hybrids – adding further to the confusion. In the present report supercapacitors are such hybrid devices, the term ultracapacitor is not used at all. Its use to designated only those devices employing pseudocapacitances seems to be a loosing proposition [6]. The statement, that B. Conway coined the term supercapacitor in 1991 is apparently erroneous. The rich collection of terms – some of them presumably protected by trademarks – does not help really: APowerCap, BestCap, BoostCap, CAP-XX, DLCAP, EneCapTen, EVerCAP, DynaCap, Faradcap, GreenCap, Goldcap, HY-CAP, Kapton capacitor, Super capacitor, SuperCap, PAS Capacitor, PowerStor, PseudoCap etc.

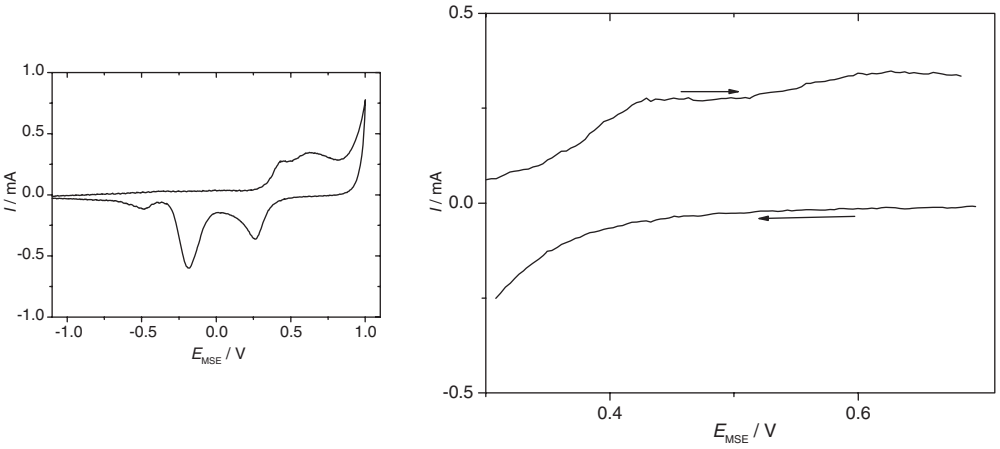

Fig. 4 CV of a polycristalline gold electrode in an aqueous electroyte solution of 0.1 **M** $KClO_4$, $dE/dt = 0.1\ V \cdot s^{-1}$, nitrogen purged.

CV curves. As already pointed out early by Conway et al. [24] the pseudocapacitance with respect to surface area may be 10 .. 100 times that of the corresponding double layer capacity – but at a cost in terms of stability and lifetime expectance because now again (electro)chemical conversions are involved.

The resulting devices are frequently also called supercapacitors. Because both principles of charge and energy storage outlined above are mixed they are more specifically called hybrid supercapacitors, actually they are one more step towards the merger of batteries and capacitors reviewed in detail elsewhere [25], for early observations see [26]. Even the carbon-based materials employed in the EDLCs may already show both features because of numerous functional groups on the carbon surface being possibly redox-reactive [27] thus bridging the gap between purely capacitive and pseudocapactive materials. Materials operating simultaneously as capacitive and pseudocapacitive storage media have sometimes also been called hybrids [25], this combination has been called parallel hybrid whereas the use in different electrodes described above has been called serial hybrid. When a pseudocapacitive electrode is combined with a double-layer type one the device is sometimes also called asymmetric. Different from the electrostatic storage mode electrochemical reactions, i.e., charge transfer and associated processes, will be involved. These interfacial reactions proceed at limited rates only (for overviews see [28–32]), the total amount of species converted (oxidized/reduced) is equivalent to the specific rate of reaction expressed as charge transfer current density $j = I/A$ (with I being the overall current and A the participating surface area) multiplied with the surface area A. Materials to be considered for application should obviously have large values of j (which in turn reflects the exchange current density j_0, for details see e.g., [33]) and/or large surface areas A. The electrode reaction actually proceeding should be a well-defined and reversible[3] like $A \leftrightarrows B$ involving preferably only a redox process and no further chemical reaction possibly associated with volume and shape change. Beyond redox processes of the type

$$MnO_2 + H_2O + e^- \leftrightarrows MnOOH + OH^- \tag{4}$$

intercalation reactions of the type

$$Li^+ + C_n + e^- \leftrightarrows LiC_n \tag{5}$$

may proceed (for a recent example see [34]). Deposition processes of species like

3 This term causes frequent confusion and is particularly ambiguous in electrochemistry. A reversible electrode reaction may be called this way because – as indicated above – conversion of the starting material A into B yields in the backward reaction exactly A. It may also be called reversible because if is very fast, actually fast enough to establish the ratio of reduced and oxidized species at the electrochemical interface according to the Nernst equation at any time, even during fast changes of the electrode potential externally impressed by e.g., a potentiostat in a cyclic voltammetry experiment. And finally it may be called reversible because it proceeds at equilibrium following the thermodynamic requirements for a reversible system.

$$H^+ + e^- \leftrightarrows H_{ad} \text{ or } Me^+ + e^- \leftrightarrows Me_{ad} \quad (6)$$

are also conceivable, their designation as electrosorption is somewhat misleading because of the easy confusion with adsorption of e.g., organic molecules [35] involving partial charge transfer [36–39] also called electrosorption.

There are further requirements active materials have to meet. They should be chemically stable in the given environment of an electrolyte solution and – a fact at least until today frequently overlooked – at elevated temperatures. This applies in particular to the chemical state the active masses reach upon charging. No chemical reaction between the "charged" material and the environment inside the cell should proceed, this would be noticed first by the user as "self-discharge" [40] and subsequently as capacity loss. This mode of self-discharge is added to those already observed in EDLCs: Redistribution of ions (charges) and leakage currents through imperfect insulations between electric leads etc. (self-discharge as a major challenge has been addressed much earlier [41], for recent work see e.g. [42–44]). First studies employing blocking layers of e.g., poly-*p*-phenyleneoxide applied to carbon surfaces have been reported, unfortunately this concept cannot be applied to pseudocapacitive electrodes [45]. Neither dissolution nor change of morphology should proceed, this includes volume change and swelling (for examples see below) which might result in cracking and poor long-term performance. The materials should be good electronic conductors because their contribution to the ESR may be substantial otherwise – and obviously not welcome. They should be cheap, abundantly available, easy to prepare and environmentally acceptable. The number of compounds meeting all these requirements appears to be limited so far. For a capacitor device always two electrodes are needed. Whereas in EDLCs the same material may be used on both sides application of redox–active materials requires a different approach. Considering the case of a metal oxide MeO_2 this becomes obvious. Assuming no higher state of oxidation than +4 is available only the reaction

$$MeO_2 + H_2O + e^- \leftrightarrows MeOOH + OH^- \quad (7)$$

is possible, for the sake of simplicity mixtures of oxides are omitted. The reduction may suggest use as a positive mass in a discharging cell. The negative mass to be combined with this electrode must show an oxidation, and assuming that the same metal should be used its reaction would be

$$MeOOH + OH^- \leftrightarrows MeO_2 + H_2O + e^- \quad (8)$$

The voltage of this device would be equivalent to the difference in electrode potential of both masses, with the actual potential of each electrode given by the ratio of the oxidized to the reduced (or less highly oxidized) species according to the Nernst equation. Obviously this ratio would be 1 in both electrodes when the device is completely discharged. And also quite obviously only 50 % of the active mass of each electrode will actually be utilized (actually in symmetric supercapacitors employing pseudocapacitive storage the utilization of the active mass is even lower). This situation has already been faced before with ICPs applied in capacitive devices with the same polymer employed in both electrodes, a device called class I (for a detailed discussion see [46]). Two solutions of this problem have emerged: Combining two different materials yields a hybrid device when one mass is based on redox processes, the other one on double layer charging (the asymmetric supercapacitor), or to combine two compounds of the the same chemical parent (element, e.g., manganese oxides) with widely different states of oxidation (the symmetric case). Another terminological approach calls all devices employing charge storage beyond the double layer hybrid devices (with the term hybrid itself being the subject of a discussion[4]) with devices employing in addition to pseudocapacitive

4 Hybrid appears to lack a proper and generally accepted definition still despite its daily use. Actually some attempts at definition consider it equal or very similar to composite. Within this text a composite will be a mixture of two components wherein the components do not interact with each other associated with any induced change of surface/interface or volume property. A hybrid will be a material where especially at the interface such interactions cause changes in properties and behavior. In this sense most examples in the published literature deal merely with composites and not with hybrids.

storage processes also double layer ones asymmetric, with the same material in both electrodes symmetric ones and with lithium-ion capacitors a third category.

As an example of the second category Mn_3O_4 (Hausmannite $Mn^{2+}Mn^{3+}Mn^{3+}O_4$), actually MnO_2, has been examined [47]. The reaction $Mn_3O_4 \rightarrow MnO_2$ performed electrochemically (see e.g., [48, 49]) is claimed to be irreversible (in the chemical sense), thus – although no electrode reactions are given – it appears likely, that during charging of the negative electrode a reduction simplified written as

$$MnO_2 + e^- + C^+ \rightarrow ([MnO_2]^- C^+) \tag{9}$$

proceeds. This may either occur only on the surface or also inside the solid, and the cations C^+ may be protons or metal ions from the electrolyte solution. In neutral electrolyte solutions composed of e.g., 1 **M** Na_2SO_4 in water the concentration of protons is more than eight orders of magnitude smaller than that of sodium ions, thus protons may justly be omitted. Somewhat confusingly attention has been mostly focussed on the adsorption (and/or insertion) of the ions on the surface in case of a truly superficial pseudocapacitive redox reaction, whereas the associated transfer of negative charge to some Mn^{4+}-ions has hardly been mentioned [50]. In this particular case the reaction may progress into the range of electrode potentials were Mn^{2+}-ions are formed irreversibly with associated losses of capacity [51].

The reaction at the positive electrode (during charging the anode) where an oxidation shall proceed during charging is harder. Most likely it is

$$([MnO_2]^- C^+) \rightarrow MnO_2 + e^- + C^+ \tag{10}$$

On discharging the supercapacitor the directions are reversed. Since both electrodes change electrochemically only slightly around basically a very similar state of oxidation the actually observed capacities tend to be small like with class I capacitors employing ICPs [46]. Instead asymmetric devices have been suggested as preferred option [52, 53]. As a minor advantage of symmetric designs simplified recycling procedures because of the less complex inventory of a cell should be kept in mind.

The most prominent and popular example is RuO_2 [54]. The redox reaction of the hydrated form (which is present when brought into contact with an acidic aqueous electrolyte solution) is

$$RuO_2 + \delta H^+ + \delta e^- \leftrightarrows RuO_{2-\delta}(OH)_\delta \text{ with } 0 < \delta < 2 \tag{11}$$

involving protons from a slightly acidic electrolyte solution or water from a neutral one [55].

$$RuO_2 + \delta H_2O + \delta e^- \leftrightarrows RuO_{2-\delta}(OH)_\delta + \delta OH^- \text{ with } 0 < \delta < 2 \tag{12}$$

The material has a high theoretical charge density of 1358 $F \cdot g^{-1}$ assuming $RuO_2 \cdot 0.5H_2O$, a sufficient electronic conductivity of $3 \cdot 10^2$ $S \cdot cm^{-1}$, electrochemical reversibility at several well defined redox steps, chemical stability etc. – and thus fulfills almost all requirements – except for price at 2.35 €·g^{-1} (8/2013), availability (it is one of the very rare elements) and toxicity[5]. Hydrated forms show significantly better performance than anhydrous ones, a feature also noteworthy with other oxides already implying the role of a solvent for the ions involved in the surface chemistry and electrochemistry. Contrary to sometimes published opinions it does not necessarily imply a major role for protons – which are present in the frequently neutral electrolyte concentrations in extremely low concentrations only. Consequently other metal oxides have been studied. Most popular is manganese dioxide, but also cobalt, copper, iron, tin, iridium and nickel oxides have been investigated. All these oxides show redox processes of the type already discussed above. Unfortunately almost no kinetic data on the redox processes of these metal oxides brought into contact with aqueous electrolyte solutions have been reported [2]. Nevertheless the subject has been addressed in a comparative study of positive masses

5 RuO_4 is particularly dangerous because it is significantly volatile.

of $Ni(OH)_2$ and $Co(OH)_2$ [56]. Although the former had a larger specific capacitance (2217 and 549 $F \cdot g^{-1}$) the latter showed higher stability of the specific capacitance and better charge/discharge efficiencies. This was attributed to the higher reversibility of the cobalt-based electrode, i.e., the faster redox kinetics. The electrode processes are generally reversible in both the chemical and presumably the electrochemical sense outlined above, the resulting compounds in various states of oxidation appear to be sufficiently stable, otherwise self discharge would be observed. Despite the dim prospects for a wide-spread use of RuO_2 itself numerous attempts to prepare composites with other metal oxides have been reported (for overviews see [5, 57]).

Further aspects require consideration. Even when assuming that intercalation or a similar reaction involving the bulk of the active mass is involved basically surface electrochemistry proceeds [58]. A rough estimate of the extent of penetration of the pseudocapacitive reaction into the volume may be gleaned from the diffusion length of participating ions derived from electrochemical impedance measurements. Horng et al. [59] have used polyaniline nanowires deposited on carbon cloth, the estimated diffusion length was 60 nm. Because the electrode performance was not limited by electrode thickness (actual diameter of the nanofibers was about 60 .. 80 nm) it has been suggested elsewhere, that the electrode reaction penetrates only a few tens of nanometers into the active mass [60]. Thus for higher rates of reaction (i.e., high currents at acceptably low current densities, i.e., high power capability of the final device) large surface areas are desirable. Attempting this by deposition in particles as fine as possible is most likely counterproductive and counterintuitive: The very fine particles may provide large surface areas, but for the reasons already outlined above a substantial fraction of this surface may simply be not accessible for electrolyte solution and ions. In addition electronic conductance of the solid phase may be too low. The stability of such deposits may also be insufficient, in addition agglomeration may proceed. There are nevertheless results obtained with electrodes prepared by simple precipitation methods, but mostly some follow-up treatment is applied. This treatment aims at a generally pursued improvement of surface distribution and sample morphology. At first glance amorphous materials may look particularly attractive because the absence of possibly large crystals prevent detrimental effects of slow solid state transport processes. There may even be a gain in cell voltage because of changes in Gibbs energy of formation when going from crystalline to amorphous materials [61]. Too small particle sizes and possibly insufficient mechanical stability have limited the success of such materials so far.

Practically all metal oxides investigated so far are wide band gap semiconductors, their electric conductance is too low for applications especially when high currents (i.e., high power) are required. Voltage losses across particles of this material may in addition cause further detrimental effects by Joule heating up to the point of serious safety concerns. Another source of increased Ohmic resistance may become more significant with decreasing particle size: The contact resistance between particles. In case of materials showing volume change and showing passivation-like surface changes this contribution may become a major one.

Various strategies have been reported to overcome or remedy the shortcomings outlined above:

- Nanostructuring with morphology controlled with respect to particle shape, particle size, pore size, particle and pore size distribution (for an overview on nanostructuring see [62])
- Deposition of thin layers (for a specific overview see [63]) on suitable structured supports fulfilling the requirements indicated in the preceding entry
- Formation of composites or hybrids[4] with materials controlling and/or maintaing advantageous properties (see again first entry) of active material during operation

Most of these strategies can be applied to materials including oxidic ones both for supercapacitor and lithium ion battery electrodes, in a review dealing with both classes of materials this has been done elsewhere [60]. Composites of metal oxides with ICPs have been reviewed elsewhere with particular attention to the role of the ICP [46]. Nanodimensional structures can be grouped as follows (with the dimensionality given in brackets):

- Nanosized columnar or wire-like arrays (nanorods, nanowires, nanofibers, nanoribbons) (1D, for a specific overview see [64], a detailed one on 1D metal oxide nanostructures see [65])
- Coated nanosized columnar or wire-like arrays (core-shell structures) with coating either protecting the active material inside or the coating being the active material on the structured support acting as current collector also

– Nanoplatelets (2D)
– Specific arrangements as nanoflowers, nanoarrays, foams (2D, 3D)

Depositing metal oxides on spherical particles or particles with an aspect ratio close to 1 would be considered 0D, use of foams or other porous structures would be 3D [66]. With respect to improved electronic conduction 2D structures show smaller contact resistance contributions than 0D particular systems, especially when prepared with their longer dimension perpendicular to the suport they are more effective. Both deposition on the outer surface of wires and deposition inside tubes may be applied. For a desired capacitance in a given volume means of preparing suitable superstructures will be required. 3D-structures may provide this means, but even their total thickness may be limited. Various routes to these products have been proposed and evaluated: Chemical formation by precipitation, sol-gel procedures, hydrothermal procedures and electrochemical deposition. Some actual procedures may incorporate steps and aspects of more than one of these basic approaches. When appraising methods and their respective products in particular of those approaches not yielding ready electrodes already effects of further preparation steps should be kept in mind. Very fine powders obtained by whatever method even when showing promising porosities etc. may behave poorly when mixed with conducting additives and binders and may pack poorly yielding finally too dense electrodes lacking the necessary meso- and even macroporosity needed for good access of electrolyte solution and ions better achieved with slightly larger, mesoporous [67] and possibly spherical particles (see examples in [68, 69]). Wire- and rod-like materials may simply fragment when exposed to mechanical pressure loosing part of the advantageous morphology.

Formation of whatever polymorph in a given particle shape (wire, tube, rod etc.) and distribution via thermal, hydrothermal or other procedures appears to be – at least initially – a trial-and-error approach. Only in some cases template-like actions of additives like the tubular growth of α-MnO_2 induced by fluoride ions (for similar cases with other metals see e.g., [70, 71]) have been identified, but even in this case only the preferred growth of certain polymorphs could be explained with different surface energies. The reasons for the growth of a particular shape were not explained. Presumably the rate of growth at different crystal planes differs substantially with the templating ions inhibiting or (less likely) accelerating at specific ones.

A combination of two materials prepared by depositing the second compound on the first one yielding a particularly intimate and effective connection between both like MnO_2 deposited onto graphene may come closest to the meaning of hybrid as indicated above, this approach has been studied most thoroughly by Wang and Die, the products are considered as strongly coupled inorganic-nano-carbon hybrids [72]. The materials obtained this way will be discussed below at the respective metal, for a review of graphene/metal oxide materials in energy storage see [73].

The materials

Following the metal oxides will be inspected more closely. Mixed oxides and metallates will be treated together with one of their constituting metals. Theoretical data are given as reported with assumed electrode reaction equation, differences and variations are mostly due to different electrode potential limits put into he calculations. Specific data, in particular those pertaining to charge, energy and power density are quoted as given by the authors. As already remarked elsewhere [52] these values tend to be of only limited meaning. Energy densities E and power densities P are sometimes calculated based on the behavior of the investigated electrode according to

$$E = \frac{1}{2} C_s (\Delta E)^2 \text{ and } P = \frac{E}{t} \text{ or } P = \frac{(\Delta E)^2}{4 \cdot ESR} \tag{13}$$

with the specific capacitance C_s, the electrode potential variation ΔE, the discharge time t taken from CVs and discharge experiments and the value of ESR derived from e.g., discharge experiments (the immediate voltage

or potential drop when switching from charge to discharge and the respective currents provide the value). Authors frequently state, that their numbers are related only to the active mass, sometimes they even distinguish between contribution of metal oxide and added carbon (for examples see [66]). Even in binder-free systems working with added conductive substances (obtained e.g., by depositing thin layers on metallic substrates) data may change dramatially when a complete device is prepared. This has been stressed before [74] taking an example with extraordinary claims regarding high energy density [75] brought back into the not-so-brilliant reality. This need for more unified reporting in particular of coulometric data has been stressed in an overview on nanomorphology control of electrode materials [62]. Reviews covering parts of the selection presented here are available [5, 76], further oxides not covered here – mostly because of very poor data – may be found elsewhere [72, 77, 78]. Because of the limitations pertaining to ruthenium this material is not considered further except for compound materials, because supplies of indium are already low this material will not be considered here (for available data see [63]).

Cobalt

Although ressources of cobalt are smaller than those of the other metals considered here attempts to prepare cobalt-based active masses have been reported. CoO_2 is not among them, because it tends to decompose releasing dioxygen – a safety issue with lithium ion batteries employing $LiCoO_2$ as positive mass during charging [79]. On selective synthesis of α- and β-$Co(OH)_2$ see [80]. Theoretical charge density has been calculated at 3560 F·g^{-1} [66] for the storage reactions

$$Co_3O_4 + OH^- + H_2O \leftrightarrows 3CoOOH + e^- \text{ and } CoOOH + OH^- \leftrightarrows CoO_2 + H_2O + e^- \quad (14)$$

Also suggested has been [81]

$$Co(OH)_2 + OH^- \leftrightarrows CoOOH + H_2O + e^- \quad (15)$$

Chou et al. [82] prepared flexible porous $Co(OH)_2$ nanoflake film deposits suitable for supercapacitor applications by a electrodeposition[6] method on lightweight and inexpensive stainless steel mesh and found it to be amorphous according to X-ray diffraction results. The maximum specific capacitance of 609.4 F·g^{-1} decreases by <5 % as the mass loading of $Co(OH)_2$ increases by more than 340 % from 0.14 to 0.62 mg·cm^{-2} assuming the redox reaction above right. The specific capacitance decreases only by <15 % when the current densities increase up to 10 times from 714 to 7143 mA·g^{-1}, indicating the good high-rate performance. Additionally, there is only 19 % specific capacitance loss after 3000 cycles, which shows the long-term electrochemical stability. After 3000 cycles, the specific capacitance of the porous $Co(OH)_2$ nanoflake electrode is 364 F·g^{-1}, which was still higher than that of carbon-based materials. Jagadale et al. [83] prepared $Co(OH)_2$ by electrodeposition during cyclic voltammetry from a 0.1 **M** $Co(NO_3)_2 \cdot 6H_2O$ solution. Presumably the same interfacial redox chemistry as observed by Chou et al. [82] prevailed. A symmetric capacitor employing two electrodes of stainless steel foil coated with $Co(OH)_2$ was assembled and tested. X-ray diffractograms taken after 5000 charge/discharge cycles indicated a higher crystallinity of the β-$Co(OH)_2$ deposit based on sharper and more intense diffraction peaks. The authors assign the redox reaction $Co(OH)_2 + OH^- \leftrightarrows CoOOH + H_2O + e^-$ to the positive electrode, whereas at the negative electrode only adsorption of potassium ions during charging/their release during discharging is claimed. The performance data for the complete cell were 44 F·g^{-1}, 3.96 Wh·kg^{-1} and 42 kW·kg^{-1}. In a study of the effect of the scan rate in potentiodynamic deposition of β-$Co(OH)_2$

6 Deposition proceeded from an aqueous solution of 0.025 **M** $Co(NO_3)_2$. Reduction of nitrate to nitrite according to $NO_3^- + H_2O + 2e^- \rightarrow NO_2^- + 2\ OH^-$ and alternatively a more complete reduction according to $NO_3^- + 7\ H_2O + 8\ e^- \rightarrow NH_4^+ + 10\ OH^-$ both yield hydroxyl ions. In the neutral, unbuffered solution the local concentration of these ions may be large enough for the precipitation reaction to occur: $Co^{2+} + 2\ OH^- \rightarrow Co(OH)_2\downarrow$.

on flexible stainless steel sheets Jagadale et al. [84] observed declining particle size and increasing porosity with growing scan rate as would be expected from metal deposition theory [85]. The material deposited at the highest scan rate of 200 $mV \cdot s^{-1}$ showed 890 $F \cdot g^{-1}$ in 1 **M** KOH electrolyte at $dE/dt = 5\ mV \cdot s^{-1}$ with a capacity loss of 16 % after 10000 cycles. A non-thermal chemical synthesis of amorphous thin films of CoO has been reported [86], the films have not been studied for supercapacitor applications. The inherent limitations set by the low conductivity have been illustrated by a comparison between a symmetric (CNT/CNT) and an asymmetric miniature capacitor [87] employing a positive α-$Co(OH)_2$/CNT and a negative CNT electrode. At 20 $A \cdot g^{-1}$ and a voltage window of 1.8 V the asymmetric device showed 62.6 $F \cdot g^{-1}$, the symmetric only 8.7 $F \cdot g^{-1}$. Because of the slightly lower ESR of the symmetric device at 30 $A \cdot g^{-1}$ its power density was 20.6 $kW \cdot kg^{-1}$ and energy density 2.2 $Wh \cdot kg^{-1}$, whereas the asymmetric device showed only 11.4 $kW \cdot kg^{-1}$ and 7.8 $Wh \cdot kg^{-1}$. Hierarchically structured Co_3O_4 has shown 781 $F \cdot g^{-1}$ at 0.5 $A \cdot g^{-1}$ and 611 $F \cdot g^{-1}$ at 8 $A \cdot g^{-1}$ with 97.8 % capacitance retention after 1000 cycles at 8 $A \cdot g^{-1}$ F [88].

The advantageous properties of hybrid materials [89] already addressed above have been employed by Liang et al. in a hybrid of Co_3O_4 with a 1D nanoporous carbon material prepared via pyrolysis of a polymeric precursor [90]. A specific capacitance of 1066 $F \cdot g^{-1}$ was reported. Mesoporous nanowires of Co_3O_4 showed substrate (e.g., carbon fiber paper or graphitized carbon paper) dependent self-organozation yielding materials with 1525 $F \cdot g^{-1}$ and 1199 $F \cdot g^{-1}$, respectively, at 1 $A \cdot g^{-1}$ [91]. A 3D material was prepared from graphene foam with Co_3O_4 nanowires deposited hydrothermally [92]. A specific capacitance of 187.1 $F \cdot g^{-1}$ was recorded at $dE/dt = 2\ mV \cdot s^{-1}$, the capacity dropped by 20 % at $dE/dt = 100\ mV \cdot s^{-1}$. Graphene-$Co(OH)_2$ nanocomposites prepared by Chen et al. [93] showed a specific capacitance of 972.5 $F \cdot g^{-1}$ at 0.5 $A \cdot g^{-1}$ (for comparison: $Co(OH)_2$ 137.6 $F \cdot g^{-1}$).

Although cobalt has been added to the nickel oxide-based electrode in alkaline secondary batteries of the Ni-MH-type [94] for quite some time providing various improvement features its redox (electro)chemistry, in particular the oxidation from $Co(OH)_2$ to CoOOH, has been understood only incompletely [95]. The reaction is a two-step process starting with a dissolution reaction of $Co(OH)_2$ followed by a solid-state step of CoOOH deposition with results sensitively depending on chemical environment and reaction conditions. β-CoOOH is the product, but varied conditions may result in formation of Co_3O_4. These findings may be helpful in understanding both formation and redox electrochemistry of cobalt-based supercapacitor electrodes.

Mai et al. [96] have prepared a hierarchical nanowire-shaped material based on a backbone of $MnMoO_4$ coated with $CoMoO_4$ showing a cycling efficiency as a high as 98 % after 1000 cycles. A composite of zeolite Y with $Co(OH)_2$ and $Ni(OH)_2$ showed a specific capacitance of 479 $F \cdot g^{-1}$ (or 1710 $F \cdot g^{-1}$ with respect to the metal content) [81]. A layered double hydroxide LDH $Co_{0.72}Ni_{0.28}$LDH had a specific capacitance of 2104 $F \cdot g^{-1}$ at 1 $A \cdot g^{-1}$ [97].

Copper

CuO nanosheets have been doped with silver by Huang et al. [98] and tested in an aqueous electrolyte solution of 6 **M** KOH yielding 689 $F \cdot g^{-1}$ at 1 $A \cdot g^{-1}$ and 299 $F \cdot g^{-1}$ at 10 $A \cdot g^{-1}$ with 61 % of the initial capacity after 2000 cycles. A composite of with porous CuO nanobelts with SWCNT in an organic solvent-based electrolyte solution showed 150 $F \cdot g^{-1}$ at 1 $A \cdot g^{-1}$ (1.25 $kW \cdot kg^{-1}$ and 130.2 $Wh \cdot kg^{-1}$, for comparison: with carbon black 127 $F \cdot g^{-1}$, even less than plain CuO with 130 $F \cdot g^{-1}$), at 24 $F \cdot g^{-1}$ at 40 $A \cdot g^{-1}$, at 5 $A \cdot g^{-1}$ it dropped from 75.7 $F \cdot g^{-1}$ to 62.4 $F \cdot g^{-1}$ (with support) [99].

Iron

α-Fe_2O_3 is an obvious candidate because of good availability, low price and lack of negative environmental impact. Low electronic conductivity is the first hurdle for application. Use of thin films may overcome this hindrance. Magnetite Fe_3O_4 shows pseudocapacitive behavior in an electrolyte solution of alkali sulfites. A film with regular octadecahydral morphology prepared hydrothermally showed a specific capacitance of

118.2 $F \cdot g^{-1}$ and a capacity retention of 88.8 % after 500 cycles [100]. With an electrolyte of Na_2SO_4 an even lower capacity of 5.3 $F \cdot g^{-1}$ was reported [101], it was assigned to the space-charge capacitance of the semiconducting oxide. With hydroxide- and phosphate-based electrolytes slightly larger values around 7 $F \cdot g^{-1}$ were recorded implying a small pseudocapacitive contribution. With Na_2SO_3 capacities ranging from 30 .. 510 $F \cdot g^{-1}$ were observed. Present data imply still insufficient electronic conductance even of composite materials with either Fe_2O_3 or Fe_3O_4, low stability and inattractive specific capacitance. Addition of MWCNT may also alleviate the effects of low conductance. An asymmetric device with at MWCNT negative and a MWCNT/α-Fe_2O_3 composite positive electrode showed energy/power densities of 50 $Wh \cdot kg^{-1}$ and 1 $kW \cdot kg^{-1}$ [102]. Presumably due to the still poor conductance and slow kinetics of the electrode reaction the capacitance dropped by 90 % from 100 to 8 $F \cdot g^{-1}$ when the scan rate was increased from 2 to 200 $mV \cdot s^{-1}$. In a microwave-assisted procedure Du et al. [103] prepared nanoparticles of Fe_3O_4. Subsequently mixed with AC symmetric and asymmetric supercapacitors were built with the asymmetric device yielding best performance in terms of cell voltage 1.2 V and energy density 9.25 $Wh \cdot kg^{-1}$ at 0.2 $mA \cdot cm^{-2}$, 53.4 % heigher than the energy density of the AC/AC-device. Hollow-sphere and colloidal $MnFe_2O_4$ have been synthesized [104], improved performance (albeit at a low level) was observed after addition of surfactants. This was attributed to lower interfacial tension and enhanced diffusion of electrolyte cations (Li^+).

A rather different picture emerges with hybrids of FeO_x and graphene. These materials show redox potentials associated with the pseudocapacitive processes at rather negative values, thus the materals may be utilized as negative masses. Qu et al. [105] prepared nanorods of FeOOH on graphene yielding a reversible Fe_3O_4-graphene electrode with a capacitance of ~320 $F \cdot g^{-1}$ stable over 1000 galvanostatic cycles in aqueous 1 **M** LiOH solution. Nanoparticles of Fe_3O_4 attached to reduced graphene oxide [106] yielded a capacitance of 480 $F \cdot g^{-1}$ at 5 $A \cdot g^{-1}$ with a corresponding energy density of 67 $Wh \cdot kg^{-1}$ at a power density of 5.5 $kW \cdot kg^{-1}$ in 1 **M** KOH solution without any decrease of capacitance after 1000 cycles.

The FeO_x-graphene hybrid reported by Wang et al. [107] combined with a Ni(OH)-graphene to a superior system is discussed below in the section on nickel. Thus the generalized statement in [5] regarding the dim prospects Fe_2O_3 or Fe_3O_4 may be somewhat precipitously.

Manganese

Manganese is abundant in nature, its compounds – especially those considered following – are environmentally acceptable and of low – if at all – toxicity. Manganese dioxide MnO_2 occurs in many forms in nature (for details see e.g., [108]). Among them are hollandite α-MnO_2, pyrolusite β-MnO_2 (rutile structure), birnessite $(Na_{0.3}Ca_{0.1}K_{0.1})(Mn^{4+},Mn^{3+})_2O_4 \cdot 1.5\ H_2O$ forming together with many other layered manganese dioxides the group of δ-MnO_2 with a layered structure [109] particularly useful for ion intercalation, akhtenskite (ε-MnO_2), ramsdellite or nsutite γ-MnO_2 or R-MnO_2 (this assignment seems to be under dispute, see e.g., [110–113]). Of interest as a precursor is also hausmannite $Mn^{2+}Mn^{3+}Mn^{3+}O_4$, although it is itself electrochemically inactive. λ-MnO_2 is a spinel phase, a-MnO_2 is an amorphous product. Lithiated forms also considered have spinel ($LiMn_2O_4$), orthorhombic or layered form ($LiMnO_2$). In numerous reports observed X-ray diffraction data taken from natural minerals are used to assign synthetic products to any of the names of naturally accuring forms, causing sometimes minor confusion. α-, β-, and R-MnO_2 show hexagonal closest packing with tunnel structures possibly useful for ion ingress/egress. γ-MnO_2 has been claimed to the electrochemically most active one [112, 114] for alkaline battery applications. It shows a thickness change of a film prepared by electrodeposition of up to 150 μm thickness by about 10 % upon reduction as measured by ellipsometry [112]. An early review of MnO_2 in supercapacitors is available [115], the state of development of asymmetric supercapacitors utilizing MnO_2 has been reported before [116, 117], and for an overview on this class of materials see also [118]. As already implied by the Pourbaix diagram of manganese [119–121] several redox transitions are possible within the stability window of water: Mn(II)/Mn(III), Mn(III)/Mn(IV), Mn(IV)/Mn(VI). Because of the numerous structural and compositional variations as well as possible redox transitions numbers of theoretical charge density vary from 1100 .. 1300 $F \cdot g^{-1}$ [5] up to 1370 $F \cdot g^{-1}$ [52] and 1380 $F \cdot g^{-1}$ [66]. In the absence of kinetic

data for the conceivable redox reactions (see above) any general statement claiming a too low reversibility seems to be unfounded [63]. This also applies to electronic conductance: Although basically a wide band gap semiconductor conductivities of up to 10^{-6} S·cm^{-1} have been quoted [52].

A major challenge in the use of MnO_2 is obviously the low (or almost absent) conductivity. This is confirmed by observations of very large specific capacitance values reaching 700 to 1380 F·g^{-1} [116] with ultrathin films (for a typical example see 698 F·g^{-1} at dE/dt = 50 mV·s^{-1} reported by Pang et al. [122], for an overview see [63]) implying both the large gain available when drastically shortening the pathway for electrons and also indicating, that slow solid state diffusion may be a problem alleviated this way. A specific capacitance of 256 F·g^{-1} at dE/dt = 50 mV·s^{-1} [123], results obtained via deposition of a metallic film of manganese subsequently oxidized yielding 214 F·g^{-1} at dE/dt = 5 mV·s^{-1} [124] or a capacitance of 279 F·g^{-1} at dE/dt = 2 mV·s^{-1} [125] do not suggest real progress. Thus nanostructuring without or with employing a support or scaffold of highly conducting material providing also a large surface area in contact with the electrolyte solution is the approach. Mesoporous MnO_2 prepared by a chemical deposition routine showed a specific capacitance of 173 F·g^{-1} at 0.25 A·g^{-1} and 123 F·g^{-1} at 4 A·g^{-1} with 93.8 % capacitance retention after 10 000 cycles [126], for a sol-gel synthesis of mesoporous MnO_2 see [127]. Wang et al. [128] obtained a highly ordered nanowire array of α-MnO_2 with a specific capacitance of 165 F·g^{-1}. Li et al. [129] used vertically aligned carbon nanofibers in a brush-like array coated in core-shell fashion with MnO_2. The measured specific pseudocapacitance of 313 F·g^{-1} added to the double layer capacitance of 36 F·g^{-1} at dE/dt = 50 mV·s^{-1}, these values kept constant up to 2 V·s^{-1}. A maximum total specific capacitance of 365 F·g^{-1} was observed at a thickness of the film of ~7.5 nm. Performance data of 32.5 Wh·kg^{-1} and 6.216 kW·kg^{-1} at a drop in capacitance of 11 % after 500 cycles were derived from CV and galvanostatic cycling experiments. Wu et al. employed a slightly different approach when depositing needle-like α-MnO_2 on a carbon fiber fabric [130]. In an aqueous electrolyte solution of 1 **M** Na_2SO_4 a specific capacitance 432 F·g^{-1} at 5 A·g^{-1} was observed. From CV data it was tentatively deduced, that sodium ions may penetrate only into the topmost layers whereas protons – despite the fact, that they are present in a concentration many orders of magnitude lower – may also reach the interior of the film. Given the typical dimension of 5 nm derived from X-ray diffraction this question may need further elaboration. Nanorods of α-MnO_2 prepared by Qu et al. [131] yielded a material of superior electrochemical cycling stability showing the influence of alkali metal ions of the employed neutral electrolyte solution on capacitance and power performance. The largest ions (K^+) resulted in highest power density, the smallest ions (Li^+) provided additional capacitance due to ion intercalation beyond surface processes. CNT nanotubes were used both as scaffold and reductand in preparation of a CNT-MnO_2 composite by Jin et al. [132]. The product showed a very high surface specific capacitance of 5.07 F·cm^{-2}. Carbon-coated CNTs further loaded with MnO_2 by Wang et al. [133] showed a maximum 227 F·g^{-1} at 0.2 A·g^{-1} at 94 % capacity retention after 1000 cycles. With super-aligned CNT arrays proposed by Zhou et al. [134] (further details see below) at a loading of 60 %wt. of Mn_2O_3 a specific capacitance of 508 F·g^{-1} being equivalent to 370 F·cm^{-3} at dE/dt = 10 mV·s^{-1} was reported. Estimated energy density was 30 Wh·kg^{-1}, power density 60 kW·kg^{-1}. Core-shell nanowires of Co_3O_4@MnO_2 showed in 1 **M** LiOH solution a specific capacitance of 480 F·g^{-1} at 2.67 A·g^{-1} with only 2.7 % capacitance loss after 5000 cycles and 56 % capacitance retention at 44.7 mA·cm^{-2} compared to 4 mA·cm^{-2} [135]. SnO_2 nanowires coated with amorphous MnO_2 showed 637 F·g^{-1} at dE/dt = 50 mV·s^{-1} (800 F·g^{-1} at 1 A·g^{-1}) in a solution of 1 **M** Na_2SO_4 at 1.2 % capacity loss after 2000 cycles [136]. In a presumably less expensive approach porous MnO_2 was synthesized by an interfacial reaction and yielded (with added acetylene black) specific capacitances ranging from 8 .. 261 F·g^{-1} in a solution of 0.5 **M** K_2SO_4 with only 3 % loss after 1300 cycles. A mixture of very thin flowerlike δ-MnO_2 with AC yielded an electrode with a specific capacitance of 85.8 F·g^{-1}, an energy density of 47.4 Wh·kg^{-1} at a power density of 200 kW·kg^{-1} and a capacity retention of 90 % after 1000 cycles in 1 **M** Na_2SO_4 solution [137]. Nanospheres of birnessite-typ MnO_2 showed 210 F·g^{-1} at 0.2 A·g^{-1} in 1 **M** Na_2SO_4 solution [138]. Nanotubes of δ-MnO_2 prepared by a hydrothermal route [139] yielded with added graphite a material showing a specific capacitance of 350 F·g^{-1} at very low discharge currents. Hydrothermally prepared α-MnO_2 nanotubes showed 220 F·g^{-1} at dE/dt = 5 mV·s^{-1} [140]. MnO_2 prepared by reduction with AC and grown on AC [141] showed in an asymmetric supercapacitor with an AC negative electrode 28.1 Wh·kg^{-1} at 100 W·kg^{-1} and 4.3 W·kg^{-1} at 5 kW·kg^{-1}. A hybrid of nanowire α-MnO_2 and MWCNT mounted with

an AC negative electrode into a capacitor showed 17.8 $Wh \cdot kg^{-1}$ at 400 $W \cdot kg^{-1}$ almost unchanged at 3340 $W \cdot kg^{-1}$ in a solution of 0.5 **M** Li_2SO_4 [142]. Carbon nanotubes with MnO_2 inside as well as outside have been prepared as 2D materials by Chen et al. [143]. The specific capacitance was 225 $F \cdot g^{-1}$ at $dE/dt = 2\ mV \cdot s^{-1}$, the material with MnO_2 deposited outside the nanotube showed only 144 $F \cdot g^{-1}$. Related to the manganese dioxide content the values are 1250 $F \cdot g^{-1}$ and 790 $F \cdot g^{-1}$, this was in part attributed to the fact, that inside the tubes both MnO_2 and Mn_2O_3 coexist as evidenced from Raman spectra. A further contribution arises from the higher utilization of the material caused be the particular dimensions of pores and channels in the material causing an ion desolvation or sieving effect [144, 145] enabling ion penetration into very small spaces. Metal oxides deposited directly onto functionalized surfaces of materials like graphene or MWCNT may result in hybrids with strong coupling [72], this also applies to reduced graphene oxide RGO because it contains frequently residual oxygen functionalities. RGO with urchin-like MnO_2 yielded a specific capacitance of 263 $F \cdot g^{-1}$ at 5 $mA \cdot cm^{-2}$ and 138 $F \cdot g^{-1}$ at 40 $mA \cdot cm^{-2}$ with 99 % capacity retention after 500 cycles [146].

0D-materials have been used as host and template for MnO_2. Dong et al. have deposited MnO_2 into the wall of mesoporous carbon CMK-3 [147] without noticeable blockage of the mesopores. The amorphous product provided a specific capacitance of 220 $F \cdot g^{-1}$ at $dE/dt = 5\ mV \cdot s^{-1}$ and 156 $F \cdot g^{-1}$ at $dE/dt = 50\ mV \cdot s^{-1}$ in an electrolyte solution of 2 **M** KCl. When considering the carbon content and its calculated double layer capacitance the contribution which could be assigned to the manganese fraction approached 60 % of the theoretical value calculated for the MnO_2 in an alkaline battery. Xu et al. prepared mesoporous amorphous MnO_2 using CNTs and mesoporous carbon as sacrifical reductands and templates [148]. The material prepared with the mesoporous carbon showed a superior specific capacitance 232 $F \cdot g^{-1}$ at 2.5 $mA \cdot cm^{-2}$ and 202 $F \cdot g^{-1}$ at 10 $mA \cdot cm^{-2}$ (87.4 % capacity retention) in a solution of 1 **M** Na_2SO_4, whereas the respective results for the CNT-based materials were 98 $F \cdot g^{-1}$ at 2.5 $mA \cdot cm^{-2}$ with only 72.7 % capacity retention at 10 $mA \cdot cm^{-2}$.

Materials prepared by depositing MnO_2 on a scaffold acting as current collector and as mechanical support providing a large surface area material frequently need a template. In case of hard templates their use requires additional processing steps when removing them; this may be associated with the risk of negatively affecting final properties. A template-free one-step method to obtain a scaffold of PEDOT nanowires coated with MnO_2 has been reported by Liu and Lee [149]. At constant electrode potential Mn^{2+}-ions from the electrolyte solution are anodically oxized, the hydrolysis of the ions in their higher state of oxidation yields MnO_2. It forms the core of the coaxial wire, whereas PEDOT is deposited as a shell. This is directed by ring-shaped sputtered gold electrodes used as support [150]. The PEDOT-coating supports an excellent electrochemical performance with a specific capacitance of 210 $F \cdot g^{-1}$ at 5 $mA \cdot cm^{-2}$ and 185 $F \cdot g^{-1}$ at 25 $mA \cdot cm^{-2}$. Using nickel foam as a 3D scaffold Zhao et al. [151] have prepared a CNT-MnO_x material with a high specific capacitance of 462 $F \cdot g^{-1}$ at 5 $A \cdot g^{-1}$ in a solution of 0.5 **M** Na_2SO_4 with only 3.68 % loss of capacitance after 500 cycles. Using commercial sponge coated with reduced graphene oxide and MnO_2 a material with a specific capacitance of 450 $F \cdot g^{-1}$ at $dE/dt = 2\ mV \cdot s^{-1}$ was obtained [152]; it worked up to $dE/dt = 200\ V \cdot s^{-1}$ with 90 % capacity retention after 10 000 cycles.

Because pseudocapacitive processes going beyond purely superficial ones imply ingress of ions into solid phases of the metal oxide both the structure of the crystal and size (and other properties) of the participating ions may be important. In a comparative study of sodium-doped δ-MnO_2 and commercial cryptomelane-type MnO_2 Boisset et al. [153] have concluded, that lithium salts with small anions provide best performance and stability. Sodium and potassium doped ranciéite-type MnO_2 has been synthesized with various morphologies, specific capacitances ranged from 17 .. 112 $F \cdot g^{-1}$ at $dE/dt = 2\ mV \cdot s^{-1}$ [154]. The influence of conditions in hydrothermal synthesis of α-MnO_2 has been examined [155].

Although most reports deal with preparation, characterization and performance evaluation mechanisms of capacitance loss and finally device failure have been inspected, albeit only infrequently. Hsieh et al. have studied capacity fading of MnO_2 (prepared by precipitation from solutions of $KMnO_4$ and $MnSO_4$ and structurally not characterized further) with an aqueous electroyte solution of 1 **M** NaCl [156]. Two different mechanisms were deduced. At low binder content as well as at high currents growth of transmission resistance assigned to deterioriating electric contact between MnO_2-particles and added conducting carbon was the culprit. The mechanical failure also observed and apparently closely related to the changes of electric

properties was attributed to cyclic volume changes during charging/discharging. With high binder content and/or low current the interfacial charge transfer resistance associated with the redox electrode reaction of the MnO_2 increased. The frequently invoked dissolution of MnO_2 as the cause of failure was also observed, but its extent could not explain the amount of fading. On a smaller dimension structural variations of δ-MnO_2 during charge/discharge have been studied [157]. Results show an increase of interlayer spacing on oxidation attributed to sodium ion deintercalation and subsequent replacement by water molecules associate with a slow loss of crystallinity. The specific capacitance of 145 $F \cdot g^{-1}$ was nevertheless maintained over 1100 cycles. The detrimental effect of oxygen was demonstrated with an asymmetric device (AC/MnO_2): After its careful removal stable performance in 195 000 cycles was found, lower corrosion in the absence of oxygen was identified as a major influence [158].

Lithiated manganese dioxide $LiMn_2O_4$ has been prepared by Wang et al. in a nanoporous form via a hydrothermal route starting with nanotubes of α-MnO_2 [159]. With a typical pore size of 40 .. 50 nm and a BET surface area of 9.76 $m^2 \cdot g^{-1}$ a specific capacitance of 189 $F \cdot g^{-1}$ at 0.3 $A \cdot g^{-1}$ current density were reported for its use as positive mass in a supercapacitor with an electrolyte solution of 0.5 **M** Li_2SO_4. At 12 $A \cdot g^{-1}$ the capacity decreases to 166 $F \cdot g^{-1}$, after 1500 cycles no capacity fading could be observed. Nanoporous spinel-type material of the same chemistry pepared by Wang et al. [160] showed 189 $F \cdot g^{-1}$ at 0.3 $A \cdot g^{-1}$, 166 $F \cdot g^{-1}$ at 12 $A \cdot g^{-1}$ and stable cycling performance even at highest current densities. A nanohybrid of this composition obtained in the same group [161] showed 415 $F \cdot g^{-1}$ at 0.5 $A \cdot g^{-1}$. A nanorod-like form of $LiMn_2O_4$ has been prepared by Tang et al. [162] from hydrothermally formed α-MnO_2 nanowires subsequently heat-treated, it has been identified as a positive mass with extremely fast response: The capacitance of 396 $F \cdot g^{-1}$ at a rate of 4.5 C was only slightly diminished to 348 $F \cdot g^{-1}$ at 90C and a power density of up to 14.5 $kW \cdot kg^{-1}$ with 94 % capacity retention after 1200 cycles. Microcubes of $LiMn_2O_4$ prepared by a self-templating route have shown a discharge capacity of 108 $mAh \cdot g^{-1}$ at rate 10 C, after 100 cycles this decreased to 88 $mAh \cdot g^{-1}$ [163]. With a nonaqueous electrolyte solution an asymmetric supercapacitor with a negative $LiMn_2O_4$ and a positive MnO_2/CNT electrode showed 56 $Wh \cdot kg^{-1}$ at 300 $W \cdot kg^{-1}$ [164]. A performance superior to lithium-ion containing masses was observed with $K_{0.27}MnO_2 \cdot 0.6H_2O$ [165] showing 17.6 $Wh \cdot kg^{-1}$ at a power density of 2 $kW \cdot kg^{-1}$. The stability and the lack of sensitivity against traces of dioxygen in the electrolyte solution was attributed to the lamellar morphology of the material. Nanoflakes of MnO_2 with spontaneously intercalated sodium ions having the stoichiometry $Na_{0.7}MnO_2$ and $Na_{0.91}MnO_2$ have shown specific capacitances > 1000 $F \cdot g^{-1}$ and calculated energy densities up to 110 Wh kg^{-1} with 99.9 % capacity retention after 1000 cycles [166]. The use of $NaMnO_2$ as active mass has been proposed by Qu et al. [167].

Molybdenum

Molybdite (α-MoO_3) may accommodate up to 1.5 lithium atoms per molybdenum [168] according to

$$MoO_3 + 1.5\ Li^+ + 1.5e^- \leftrightarrows Li_{1.5}MoO_3 \tag{16}$$

A mesoporous film of isooriented α-MoO_3 showed higher lithium ion storage capacity than an amorphous one, this was attributed to ion insertion into the van der Waals-gaps [169]. Nanoplates of α-MoO_3 as prepared by Tang et al. [170] as negative electrode in an asymmetric supercapacitor (with a positive electrode of AC) showing 280 $F \cdot g^{-1}$ at 1 $dE/dt = 1\ mV \cdot s^{-1}$ in aqueous 0.5 **M** Li_2SO_4 (45 $Wh \cdot kg^{-1}$ at 450 $W \cdot kg^{-1}$; 29 $Wh \cdot kg^{-1}$ at 2 $kW \cdot kg^{-1}$).

A 3D heterostructured nanowire $MnMoO_4/CoMoO_4$ was synthesized by Mai et al. [171] with a specific capacitance of 187.1 $F \cdot g^{-1}$ and 26 $Wh \cdot kg^{-1}$ at 1 $A \cdot g^{-1}$ in an aqueous solution of 2 **M** NaOH. Tubular and sheetlike nanocomposites of MoO_3 with polyaniline intercalated between layers of the oxide were prepared [172]. After about 100 cycles the sheet-like material showed a larger specific capacitance of 200 $F \cdot g^{-1}$ vs 170 $F \cdot g^{-1}$ for the tubular one. A beneficial effect of coating (α-MoO_3) with polypyrrole (see also [46]) has been attributed to efficient inhibition of molybdenum ion dissolution and improved electronic conductance of the embedding polymeric matrix [173].

Nickel

Theoretical charge density has been calculated at 2584 F·g^{-1} [66] and 3750 F·g^{-1} [7] for the storage reaction

$$NiO + OH^- \leftrightarrows NiOOH + e^- \quad (17)$$

which is equivalent to

$$Ni(OH)_2 + OH^- \leftrightarrows NiOOH + H_2O + e^- \quad (18)$$

This reaction is valid for all nickel oxides, hydroxides etc., its electrode potential is rather high and suggests the use of these materials as positive electrode. Structural and mechanistic aspects of these transitions have been studied by Wen et al. [174]. The influence of the hydrothermal deposition temperature on the morphology of β-$Ni(OH)_2$ has been studied by Gund et al. [175]; the nanoplate material prepared at the lowest temperature of 333 K provided the highest specific capacitance of 340 F·g^{-1} at 0.125 mA·cm^{-2}.

Jiang et al. prepared monodisperse peapod-like nickel particles of about 20 nm diameter inside mesoporous carbon fibers [176]. The product showed superior data: 912 F·g^{-1} at 0.5 A·g^{-1} down to 468 F·g^{-1} at 10 A·g^{-1}. A 2D material with NiO on CNT has been reported by Lee et al. [177] with a specific capacitance of 160 F·g^{-1} at 10 mA·g^{-1} dropping to 140 F·g^{-1} at 100 mA·g^{-1} stable over 100 cycles. An improved conductance caused by entangling with MWCNTs and better accessability of redox sites in nanoflakes of NiO were found by Zheng et al. [178]. At an optimum content of 20 %wt. of MWCNT a specific capacitance of 210 F·g^{-1} at 0.1 A·g^{-1} dropping to 185 F·g^{-1} at 4 A·g^{-1} with a capacity loss of 11 % after 200 cycles was found. Different morphologies of NiO changing from 2D disks to 0D mesoporous spheres in composites with CNT were obtained by Lin et al. [179]. The latter material (with 23.91 %wt. of NiO in the composite) yielded the highest specific capacitance of 1329 F·g^{-1} (with respect to NiO fraction at) at 84 A·g^{-1} in an electrolyte solution of 1 **M** KOH hardly changed within 1000 cycles. Even more effective (in particular with frequently overlooked utilization of chemicals employed in the preparation process) is the use of super-aligned CNT arrays proposed by Zhou et al. [180]. At a loading of 60 %wt. on the CNTs a specific capacitance of 363 F·g^{-1} being equivalent to 110 F·cm^{-3} at dE/dt = 10 mV·s^{-1} was reported. At a current density increased by a factor of 60 the capacitance dropped by 50 %. The weight contribution of the support in an actual device would be very low, the sheets can be stacked easily. Microwave-assisted synthesis yielded a material with a porous ball-shaped surface [181] with a specific capacitance of 420 F·g^{-1} at 0.5 A·g^{-1} and 330 F·g^{-1} at 4 A·g^{-1} without noticeable capacity loss after 400 cycles. Better crystallinity were attributed to the microwave heating causing accelerated kinetics and local overheating supporting the observed favorable aggregation, which in turn yielded a surface better accessible for hydroxyl ions during pseudocapacitive processes.

Deposition of β-$Ni(OH)_2$ platelets on graphene yielded a material with a specific capacitance of 1267 F·g^{-1} at dE/dt = 5 mV·s^{-1} in an electrolyte solution of 1 **M** KOH [182], this value decreased to 877 F·g^{-1} (per active mass only) at dE/dt = 40 mV·s^{-1}. The theoretical limit was estimated to be 1900 F·g^{-1}. During galvanostatic charging at 2.8 A·g^{-1} a capacitance of 1335 F·g^{-1} was observed, this decreased to 935 F·g^{-1} at 45.7 A·g^{-1}. This performance as well as the observed stability (no capacitance loss during 2000 cycles) was attributed to the close interactions between the metal hydroxide and the graphene and a particularly suitable size and morphology of the metal hydroxide particles. Platelets of $Ni(OH)_2$ deposited on graphene were combined with RuO_2-graphene into a device operating with an electrolyte solution of 1 **M** KOH [183]. A power density of 48 Wh·kg^{-1} at a power density of ~0.23 kW·kg^{-1} and of ~21 kW·kg^{-1} at ~14 Wh·kg^{-1} clearly outperformed a symmetric $Ru(OH)_2$ supercapacitor. This is in part caused by the higher cell voltage of ~1.5 V again strongly advocating against symmetric pseudocapacitive devices. The charge/discharge behavior seems to imply, that $Ni(OH)_2$ acts as a battery electrode and $Ru(OH)_2$ as a pseudocapacitive electrode [72]. An apparently even more effective interaction was observed when instead of graphene MWCNTs were used as a substrate [107]. The superior performance was in

7 This value quoted erroneously in [5] is unsupported.

part attributed to the undisturbed interior of the MWCNTs acting as electronic conductors, whereas the outer surface could be most suitably be chemically modified for interaction with the nickel hydroxide deposit. When combined with an FeO_x-graphene hybrid a battery-like device with 120 $Wh \cdot kg^{-1}$ and 15 $kW \cdot kg^{-1}$ was obtained. Lee et al. prepared nanoparticular α-$Ni(OH)_2$ on graphene in an ethylene glycol solution without any template [184] showing a specific capacitance of 1215 $F \cdot g^{-1}$ at $dE/dt = 5\ mV \cdot s^{-1}$ and 521 $F \cdot g^{-1}$ at $dE/dt = 50\ mV \cdot s^{-1}$. A decay by 12.1 % after 1000 CV cycles was observed although the author claimed superior electrochemical properties of α-$Ni(OH)_2$ as compared to β-$Ni(OH)_2$. Elsewhere this has been attributed to structural instabilities of α-$Ni(OH)_2$ [72]. Nanosheets of α-$Ni(OH)_2$ were assembled by Yang et al. [185] into spherical flowers on a graphene support with a specific capacitance of 1761 $F \cdot g^{-1}$ at $dE/dt = 5\ mV \cdot s^{-1}$, of 1026 $F \cdot g^{-1}$ at 5.7 $A \cdot g^{-1}$ and a slight capacitance decay after 1000 CV cycles in an electrolyte solution of 6 **M** KOH. NiO nanoparticles were prepared on graphene by Wu et al. [186] yielding a material with a capacitance of 569 $F \cdot g^{-1}$ at 5 $A \cdot g^{-1}$ (for comparison: graphene oxide electrode 13 $F \cdot g^{-1}$ and NiO electrode 45 $F \cdot g^{-1}$) and 339 $F \cdot g^{-1}$ at 30 $A \cdot g^{-1}$ for the redox reaction stated above. Zhao et al. [187] synthesized two-dimensional nanosheets of NiO on graphene with a capacitance of 525 $F \cdot g^{-1}$ at 200 $mA \cdot g^{-1}$ and a capacity retention of 95.4 % after 1000 cycles in a solution of 6 **M** KOH.

Wang et al. reported a composite of reduced graphene oxide with nickel cobaltite $NiCo_2O_4$ [188] with a specific capacitance of 835 $F \cdot g^{-1}$ at 1 $A \cdot g^{-1}$ and 615 $F \cdot g^{-1}$ at 20 $A \cdot g^{-1}$ in a solution of 6 **M** KOH. Surprisingly the former value increased with cycling number to 1050 $F \cdot g^{-1}$ after 450 cycles staying at 908 $F \cdot g^{-1}$ after 4000 cycles. $NiCo_2O_4$ was deposited as rather uniform nanocrystals (average size 3 .. 5 nm) inside a carbon aerogel by Chien et al. [189] yielding a material with 1700 $F \cdot g^{-1}$ at $dE/dt = 25\ mV \cdot s^{-1}$ and 800 $F \cdot g^{-1}$ at $dE/dt = 500\ mV \cdot s^{-1}$ in an aqueous solution of 1 **M** NaOH. A decay of 2.4 % was found after 2000 cycles.

Tin

Amorphous tin dioxide has been synthesized on stainless steel electrodes by electrodeposition from a solution of Sn^{2+}-ions by Prasad and Miura [190]. Specific capacitances of 285 $F \cdot g^{-1}$ at a scan rate of 10 $mV \cdot s^{-1}$ and 101 $F \cdot g^{-1}$ at 200 $mV \cdot s^{-1}$ were observed. Somewhat surprisingly with growing amount of oxide deposited (by growing number of potentiodynamic cycles applied during deposition) the specific capacitance increased, usually the opposite effect is expected and observed because with growing amounts of deposit utilization especially of material at the bottom of the deposit is poor. The author attribute this unexpected effect to their mode of deposition by applying fast electrode potential scans. This could indeed be the cause since at fast scan rates highly amorphous material at a high rate of nucleation resulting in a very open pore structure even at substantial thickness may be formed. Nevertheless – this would explain only a constant specific capacity, the reason for the growth may be more complicated. As no CVs have been reported it can only be speculated, that during extended potential cycling dissolution/redeposition of active mass may contribute to an advantageous change of morphology. In an electrolyte soution of 0.1 **M** NaCl a composite of SnO_2 with Al_2O_3 showed a capacitance of 119 $F \cdot g^{-1}$, much larger than the value fur plain SnO_2 in this solution [191]. A composite of Fe_3O_4-SnO_2 showed a capacitance of 33 $F \cdot g^{-1}$ (or ~130 $F \cdot cm^{-3}$) at $dE/dt = 50\ mV \cdot s^{-1}$ in 1 **M** Na_2SO_4 [192]. Channu et al. prepared nanoparticles of a SnO_2-RuO_2 composite [57] with specific capacitances approaching values found for pure RuO_2 prepared and characterized under the same conditions.

Vanadium

The numerous vanadium oxides, their structures, temperature-depending metal-to-insulator transitions and applications in energy technology (except supercapacitors) have been reviewed elsewhere [193]. Because of its layered structure V_2O_5 has attracted attention already in lithium ion battery research as a material with small negative effects of volume change. In particular amorphous materials as compared to crystalline ones have shown promising performance (see e.g., [194]). Theoretical charge density has been calculated at 2120 $F \cdot g^{-1}$ [66] for the storage reaction

$$V_2O_5 + 4M^+ 4e^- \leftrightarrows M_4V_2O_5 \quad (19)$$

Amorphous $V_2O_5$was prepared by Chen et al. using a melt-quenching method [194]. In their hybrid (asymmetric) supercapacitor employing V_2O_5 as a positive electrode and activated carbon AC as a negative at a mass ration of 1:3 the highest capacitance equal to that of a symmetric cell with both electrodes of V_2O_5. This is presumably due to the fact, that AC operates with double layer storage only.

Nanoribbons of V_2O_5 have been investigated by Qu et al. [195]. The behavior in different neutral electrolyte solutions of 0.5 **M** Li_2SO_4, Na_2SO_4, and K_2SO_4 has been compared. Lowest charge transfer resistance, most pronounced peak shape in CVs and relatively highest capacitance were observed with K_2SO_4 and attributed to the best fit between cation size and behavior and interlayer spacing. Apparently the interactions between the layers of V_2O_5 and lithium ions were too strong, sodium ions show a behavior intermediate between lithium and potassium ions. Nanorod $H_2V_3O_8$ has been synthesized and characterized by Channu et al. [196]. In an aqueous electrolyte solution of 2 **M** H_2SO_4 the material showed capacitances of 42.8 $F \cdot g^{-1}$ at dE/dt = 5 $mV \cdot s^{-1}$ and 39.2 $F \cdot g^{-1}$ at dE/dt = 10 $mV \cdot s^{-1}$. Interwoven CNT and nanofibres of V_2O_5 were reported by Chen et al. [197] with 440 $F \cdot g^{-1}$ at 0.25 $A \cdot g^{-1}$ and 200 $F \cdot g^{-1}$ at 10 $A \cdot g^{-1}$. An asymmetric supercapacitor with a MnO_2/carbon composite as positive electrode and an aqueous electrolyte solution of 1 **M** Na_2SO_4 a capacitance with respect to the total weight of materials of both electrodes of 45 $F \cdot g^{-1}$, an energy density of 16 $Wh \cdot kg^{-1}$ and a power density of 75 $W \cdot kg^{-1}$ were found. At a current corresponding to a power density 3.75 $kW \cdot kg^{-1}$ an energy density of 5.5 $Wh \cdot kg^{-1}$ was measured, more than 90 % of the initial capacitance were retained after 100 cycles. Costs of active masses were estimated to be comparable to those of materials currently employed in EDLCs. Nanorods and sol-gel films of V_2O_5 and nickel nanowires coated with V_2O_5 have been prepared by Wang and Cao [198]. The high intercalation capability and associated pseudocapacitance decrease rapidly with growing current density for the nanorods and the films whereas the core-shell nanocables could retain it. Their lithium ion intercalation capability at 1 $A \cdot g^{-1}$ is 10 times higher than the capacity of the nanorod and 20 times than of the sol-gel V_2O_5 in an electrolyte soution of 1 **M** $LiClO_4$ in propylene carbonate and decreases from 3.2 Li^+ per V_2O_5 to 2.7 at 8 $A \cdot g^{-1}$.

Concluding remarks

Among the metal oxides and related composites containing either two or more oxides or containing conductive additives some compounds show particular promise, the most prominent example is MnO_2. Because the final performance depends on numerous parameters and properties of the metal oxide, the composite, the cell and the mode of operation no simple and straightforward way to the ideal material exists. This challenging sitution is further complicated, when for a given material the pseudocapacitive and the double-layer properties are considered with an eye on utilization of both. Further research at the materials level should aim at simple, energetically attractive and highly reproducible procedures. Structural considerations of the interplay between pore volume, surface area, their distribution, electrochemically accessible surface area, electronic conductivity and the change as a function of time and operating conditions, possibly including the use of molecular modelling, should help in finding optimum crystallinity and structure starting from the lowest level. Self-discharge – a topic so far addressed only for double-layer capacitors – may merit more attention because of the possibly more complicated processes inside a pseudocapacitive device. Although most applications of supercapacitors seem to be in the very short – to short time range many possible uses as replacement of secondary batteries require charge retention times more in the range of weeks and longer.

Acknowledgments: Preparation of this report has been supported in various ways by Alexander von Humboldt-Foundation, Deutscher Akademischer Austauschdienst, Fonds der Chemischen Industrie, Deutsche Forschungsgemeinschaft, National Basic Research Program of China, and Natural Science Foundation of China. Generous hospitality of Yuping Wu and Fudan University in Shanghai/China provided the inspiring environment for writing it.

References

[1] Y. Wu, R. Holze. *Electrochemical Energy Storage and Conversion*, Weinheim, WILEY-VCH (2014).
[2] for a tabulation of further values see: R. Holze: *Landolt-Börnstein: Numerical Data and Functional Relationships in Science and Technology, New Series, Group IV: Physical Chemistry, Volume 9: Electrochemistry, Subvolume A: Electrochemical Thermodynamics and Kinetics,* W. Martienssen, M. D. Lechner Eds., Springer-Verlag, Berlin (2007).
[3] V. R. Koch. *Recent Advances in Electrolytes for Electrochemical Double Layer Capacitors*, Covalent Associates, Inc., Woburn (2005).
[4] R. Holze. Landolt-Börnstein: *Numerical Data and Functional Relationships in Science and Technology, New Series, Group IV: Physical Chemistry, Volume 9: Electrochemistry, Subvolume B: Electrochemical Conductivity Data and Related Properties,* W. Martienssen, M. D. Lechner Eds., Springer-Verlag, Berlin, in preparation.
[5] G. Wang, L. Zhang, J. Zhang. *Chem. Soc. Rev.* **41**, 797 (2012).
[6] A. Burke. *J. Power Sources* **91**, 37 (2000).
[7] J. M. Miller. *Ultracapacitor Applications*, The Institution of Engineering and Technology, London (2011).
[8] *Electrochemical Supercapacitors for Energy Storage and Delivery - Fundamentals and Applications*, A. Yu, V. Chabot, J. Zhang (Eds.), CRC Press, Boca Raton (2013).
[9] F. Lufrano, P. Staiti. *Int. J. Electrochem. Sci.* **4**, 173 (2009).
[10] B. E. Conway. *Electrochemical Supercapacitors: Scientific Fundamentals and Technological Applications*, Springer, New York (1999).
[11] J. M. Miller. *Ultracapacitor Applications*, The Institution of Engineering and Technology, London 2011.
[12] *Electrochemical Supercapacitors for Energy Storage and Delivery - Fundamentals and Applications*, A. Yu, V. Chabot, J. Zhang (Ed.), CRC Press, Boca Raton (2013).
[13] D. Qu, H. Shi. *J. Power Sources* **74**, 99 (1998).
[14] H. I. Becker. US-Patent US2800616, 23.07.1957.
[15] R. A. Rightmire. US-Patent US3288641, 29.11.1966.
[16] W. Schmickler, D. Henderson. *Prog. Surf. Sci.* **22**, 323 (1986).
[17] E. Frackowiak, G. Lota, J. Machnikowski, C. Vix-Guterl, F. Beguin. *Electrochim. Acta* **51**, 2209 (2006).
[18] O. Barbieri, M. Hahn, A. Herzog, R. Kötz. *Carbon* **43**, 1303 (2005).
[19] R. Holze. *Experimental Electrochemistry: A Laboratory Textbook*, VCH-Wiley, Weinheim (2009).
[20] B. E. Conway, W. G. Pell. *J. Solid State Electrochem.* **7**, 637 (2003).
[21] L. D. Burke, D. T. Buckley, J. A. Morrissey. *Analyst* **119**, 841 (1994).
[22] B. E. Conway, E. Gileadi. *Trans. Faraday Soc.* **58**, 2493 (1962).
[23] J. Heinze, J. Mortensen, M. Störzbach. in: Springer Series in Solid State Sci. 76, H. Kuzmany, M. Mehring and S. Roth (Eds.), p. 385, Springer-Verlag, Berlin (1987).
[24] B. E. Conway, V. Birss, J. Wojtowicz. *J. Power Sources* **66**, 1 (1997).
[25] D. Cericola, R. Kötz. *Electrochim. Acta* **72**, 1–17 (2012) .
[26] B. E. Conway. *J. Electrochem. Soc.* **138**, 1539 (1991).
[27] R. Holze. 4th Carbon Conference Baden-Baden, Germany, 30.06.-04.07.1986, Ext.Abstr., p. 361.
[28] K. J. Vetter, S. Bruckenstein. *Electrochemical kinetics*. Academic Press, New York (1967).
[29] R. J. Dwayne Miller, G. L. McLendon, A. J. Nozik, W. Schmickler, F. Willig.*Surface Electron Transfer Processes*, VCH Publishers, Inc., New York (1995).
[30] W. Schmickler, E. Santos. *Interfacial Electrochemistry*, Springer-Verlag, Heidelberg (2010).
[31] N. B. Luque, W. Schmickler. *Electrochim. Acta* **88**, 892 (2013).
[32] C. Batchelor-McAuley, E. Laborda, M. C. Henstringe, R. Nissim, R. G. Compton. *Electrochim. Acta* **88**, 895 (2013).
[33] J. O' M. Bockris, A. K. N. Reddy. *Modern Electrochemistry 2A. Fundamentals of Electrodics*, 2nd ed., Kluwer, Dordrecht (2001).
[34] V. Augustyn, J. Come, M. A. Lowe, J. W. Kim, P. -L. Taberna, S. H. Tolbert, H. D. Abruña, P. Simon, B. Dunn. *Nature Mat.* **12**, 518 (2013).
[35] B. B. Damaskin, O. A. Petrii, V. V. Batrakov. *Adsorption organischer Verbindungen an Elektroden*, Akademie-Verlag, Berlin (1975).
[36] D. Rolle, J. W. Schultze. *J. Electroanal. Chem.* **229**, 141 (1987).
[37] D. Rolle, J. W. Schultze. *Electrochim. Acta* **31**, 991 (1986).
[38] F. D. Koppitz, J. W. Schultze, D. Rolle. *J. Electroanal. Chem.* **170**, 5 (1984).
[39] K. J. Vetter, J. W. Schultze. *Ber. Bunsenges. Phys. Chem.* **76**, 920 (1972).
[40] A. Lewandowski, P. Jakobczyk, M. Galinski, M. Biegun. *Phys. Chem. Chem. Phys.* **15**, 8692 (2013).
[41] H. Chen, T. N. Cong, W. Yang, C. Tan, Y. Li, Y. Ding. *Prog. Nat. Sci.* **19**, 291 (2009).
[42] S. Ban, J. Zhang, L. Zhang, K. Tsaya, D. Song, X. Zou. *Electrochim. Acta* **90**, 542 (2013).
[43] Q. Zhang, J. Rong, D. Ma, B. Wei. *Energy Environm. Sci.* **4**, 2152 (2011).
[44] A. M. Oickle, H. A. Andreas. *J. Phys. Chem. C* **115**, 4283 (2011).

[45] T. Tevi, H. Yaghoubi, J. Wang, A. Takshi. *J. Power Sources* **241**, 589 (2013).
[46] R. Holze, Y. Wu. *Electrochim. Acta*, in press, DOI: http://dx.doi.org/10.1016/j.electacta.2013.08.100.
[47] D. P. Dubal, A. D. Jagadale, C. D. Lokhande. *Electrochim. Acta* **80**, 160 (2012).
[48] D. P. Dubal, D. S. Dhawale, R. R. Salunkhe, C. D. Lokhande. *J. Electrochem. Soc.* **157**, A812 (2010).
[49] D. P. Dubal, D. S. Dhawale, R. R. Salunkhe, C. D. Lokhande. *J. Electroanal. Chem.* **647**, 60 (2010).
[50] L. Athouël, F. Moser, R. Dugas, O. Crosnier, D. Bélanger, T. Brousse. *J. Phys. Chem. C* **112**, 7270–7277 (2008) .
[51] E. Raymundo-Piñero, V. Khomenko, E. Frackowiak, F. Béguina. *J. Electrochem. Soc.* **152**, A229 (2005).
[52] G. Yu, X. Xie, L. Pan, Z. Bao, Y. Cui. *Nano Energy* **2**, 213 (2013).
[53] V. Khomenko, E. Raymundo-Piñero, E. Frackowiak, F. Béguina. *Appl. Phys. A* **82**, 567 (2006).
[54] S. Trasatti, G. Buzzanca. *J. Electroanal. Chem.* **29**, A1 (1971).
[55] J. R. Miller, P. Simon. *Science* **321**, 651 (2008).
[56] C. -C. Hu, J. -C. Chen, K. -H. Chang. *J. Power Sources* **221**, 128 (2013).
[57] V. S. Reddy Channu, R. Holze, S. A. Wicker Sr., E. H. Walker Jr., Q. L. Williams, R. R. Kalluru. *Mat. Sci. Appl.* **2**, 1175 (2011).
[58] J. O' M. Bockris, S. U. M. Khan. *Surface Electrochemistry*. Plenum Press, New York (1993).
[59] Y. -Y. Horng, Y. -C. Lu, Y. -K. Hsu, C. -C. Chen, L. -C. Chen, K. -H. Chen. *J. Power Sources* **195**, 4418 (2010).
[60] J. Jiang, Y. Li, J. Liu, X. Huang, C. Yuan, X.W. Lou, *Adv. Mater.* **24**, 5166 (2012).
[61] O. Delmer, P. Balaya, L. Kienle, J. Mayer. *Adv. Mater.* **20**, 501 (2008).
[62] S. Chen, W. Xing, J. Duan, X. Hu, S. Z. Qiao. *J. Mater. Chem. A* **1**, 2941 (2013).
[63] C. D. Lokhande, D. P. Dubal, O. -S. Joo. *Curr. Appl. Phys.* **11**, 255 (2011).
[64] D. Zhao, Y. Wang, Y. Zhang. *Nano-Micro Lett.* **3**, 62 (2011).
[65] R. S. Devan, R. A. Patil, J. -H. Lin, Y. -R. Ma. *Adv. Funct. Mat.* **22**, 3326 (2012).
[66] M. Zhi, C. Xiang, J. Li, M. Li, N. Wu. *Nanoscale* **5**, 72 (2013).
[67] H. Jiang, J. Ma, C. Li. *Adv. Mater.* **24**, 4197 (2012).
[68] J. Qian, M. Zhou, Y. Cao, X. Ai, H. Yang. *J. Phys. Chem. C* **114**, 3477 (2010).
[69] J. Liu, T. E. Conry, X. Song, L. Yang, M. M. Doeff, T. J. Richardson. *J. Mater. Chem.* **21**, 9984 (2011).
[70] N. K. Allam, M. A. El-Sayed. *J. Phys. Chem. C* **114**, 12024 (2010).
[71] W. Wei, K. Lee, S. Shaw, P. Schmuki. *Chem. Commun.* **48**, 4244 (2012).
[72] H. Wang, H. Dai. *Chem. Soc. Rev.* **42**, 3088 (2013).
[73] Z. -S. Wu, G. Zhou, L. -C. Yin, W. Ren, F. Li, H. -M. Cheng. *Nano Energy* **1**, 107 (2012).
[74] Y. Gogotsi, P. Simon. *Science* **334**, 917 (2011).
[75] C. Liu, Z. Yu, D. Neff, A. Zhamu, B. Z. Jang. *NanoLett* **10**, 4863 (2010).
[76] W. Deng, X. Ji, Q. Chen, C. E. Banks. *RSC Advances* **1**, 1171 (2011).
[77] A. K. Mishra. S. Ramaprabhu. *J. Phys. Chem. C* **115**, 14006 (2011).
[78] C. Hu, Y. -H. Huang, K. -H. Chang. *J. Power Sources* **108**, 117 (2002).
[79] R. A. Huggins. *J. Electrochem. Soc.* **160**, A3001 (2013).
[80] Z. Liu, R. Ma, M. Osada, K. Takada, T. Sasaki. *J. Am. Chem. Soc.* **127**, 13869 (2005).
[81] Y. -Y. Liang, S. -J. Bao, H. -L. Lin. *J. Solid State Electrochem.* **11**, 571 (2007).
[82] S. L. Chou, J. Z. Wang, H. K. Liu, S. X. Dou. *J. Electrochem. Soc.* **155**, A926 (2008).
[83] A. D. Jagadale, V. S. Kumbhar, D. S. Dhawale, C. D. Lokhande. *Electrochim. Acta* **98**, 32 (2013).
[84] A. D. Jagadale, V. S. Jamadade, S. N. Pusawale, C. D. Lokhande. *Electrochim. Acta* **78**, 92 (2012).
[85] E. Budevski, G. Staikov, W. J. Lorenz. *Electrochemical Phase Formation and Growth*, VCH, Weinheim (1996).
[86] S. G. Kandalkar, C. D. Lokhande, R. S. Mane, S. -H. Han. *Appl. Surf. Sci.* **253**, 3952 (2007).
[87] C. -H. Chen, D. -S. Tsai, W. -H. Chung, K. -Y. Lee, Y. -M. Chen, Y. -S. Huang. *J. Power Sources* **204**, 510 (2012).
[88] Y. Xiao, S. Liu, F. Li, A. Zhang, J. Zhao, S. Fang, D. Jia. *Adv. Funct. Mater.* **22**, 4052 (2012).
[89] for some rather general remarks see: P. Gomez-Romero, O. Ayyad, J. Suarez-Guevara, D. Munoz-Rojas. *J. Solid State Electrochem*. **14**, 1939 (2010).
[90] Y. Liang, M. G. Schwab, L. Zhi, E. Mugnaioli, U. Kolb, X. Feng, K. Müllen. *J. Am. Chem. Soc.* **132**, 2010 (15030).
[91] R. B. Rakhi, W. Chen, D, Cha, H. N. Alshareef. *Nano Lett.* **12**, 2559 (2012).
[92] X. -C. Dong, H. Xu, X. -W. Wang, Y. -X. Huang, M. B. Chan-Park, H. Zhang, L. -H. Wang, W. Huang, P. Chen. *ACS Nano 6*, 3206 (2012).
[93] S. Chen, J. Zhu, X. Wang. *J. Phys. Chem. C* **114**, 11829 (2010).
[94] *Linden's Handbook of Batteries*, T. B. Reddy Ed., 4th ed., McGraw Hill, New York (2011).
[95] V. Pralong, A. Delahaye-Vidal, B. Beaudoin, B. Gérand, J. -M. Tarascon. *J. Mater. Chem.* **9**, 955 (1999).
[96] L. -Q. Mai, F. Yang, Y. -L. Zhao, X. Xu, L. Xu, Y. -Z. Luo. *Nature Comm.* **2**, 381 (2011).
[97] V. Gupta, S. Gupta, N. Miura. *J. Power Sources* **175**, 680 (2008).
[98] J. Huang, H. Wu, D. Cao, G. Wang. *Electrochim. Acta* **75**, 208 (2012).
[99] X. Zhang, W. Shi, J. Zhu, D. J. Kharistal, W. Zhao, B. S. Lalia, H. H. Hng, Q. Yan. *ACS Nano* **5**, 2013 (2011).
[100] J. Chen, K. Huang, S. Liu. *Electrochim. Acta* **55**, 1 (2009).
[101] N. L.Wu, S. Y.Wang, C. Y. Han, L. R. Shiue. *J. Power Sources* **113**, 173 (2003).
[102] X. Zhao, C. Johnston, P. S. Granta. *J. Mater. Chem.* **19**, 8755 (2009).

[103] X. Du, C. -Y. Wang, M. -M. Chen, Y. Jang. *J. Inorg. Mater.* **23**, 1193 (2008).
[104] B. Wang, P. Guo, H. Bi, Q. Li, G. Zhang, R. Wang, J. Liu, X.S. Zhao. *Int. J. Electrochem. Sci.* **8**, 8966 (2013).
[105] Q. Qu, S. Yang, X. Feng. *Adv. Mater.* **23**, 5574 (2011).
[106] W. Shi, J. Zhu, D. H. Sim, Y. Y. Tay, Z. Lu, X. Zhang, Y. Sharma, M. Srinivasan, H. Zhang, H. H. Hng, Q. Yan. *J. Mater. Chem.* **21**, 3422 (2011).
[107] H. Wang, Y. Liang, M. Gong, Y. Li, W. Chang, T. Mefford, J. Zhou, J Wang, T. Regier, F. Wei, H. Dai. *Nat. Commun.* **3**, 917 (2012).
[108] *Handbook of Mineralogy*, J.W. Anthony, R.A. Bideaux, K.W. Bladh, M.C. Nichols, Eds., Mineralogical Society of America, Chantilly, VA 20151-1110, USA. http://www.handbookofmineralogy.org/.
[109] S. W. Donne, A. F. Hollenkamp, B. C. Jones. *J. Power Sources* **195**, 367 (2010).
[110] C. Wu, W. Xie, M. Zhang, L. Bai, J. Yang, Y. Xie. *Chem. Eur. J.* **15**, 492 (2009).
[111] W. Kucza. *Electrochem. Comm.* **4**, 669 (2002).
[112] M. Hernández Ubeda, M. A. Pérez, H. T. Mishima, H. M. Villullas, J. O. Zerbino, B. A. López de Mishima, M. López Teijelo. *J. Electrochem. Soc.* **152**, A37-A41 (2005).
[113] http://www.mindat.org/
[114] see also: C. Wu, W. Xie, M. Zhang, l. Bai, J. Yang, Y, Xie. *Chem. Eur. J.* **15**, 492 (2009).
[115] S. W. Zhang, G. Z. Chen. *Energ. Mat.* **3**, 186 (2008).
[116] D. Bélanger, T. Brousse, J. W. Long. *The Electrochemical Society Interface* **17**(1), 49 (2008).
[117] W. Wei, X. Cui, W. Chen, D. G. Ivey. *Chem. Soc. Rev.* **40**, 1697 (2011).
[118] Handbook of Battery Materials (C. Daniel, J.O. Besenhard Eds.), p. 89. Wiley-VCH, Weinheim (2011).
[119] M. Pourbaix. *Atlas of Electrochemical Equilibria in Aqueous Solutions*, Pergamon Press, Brussels (1966); M. Pourbaix: *Atlas of electrochemical equilibria in aqueous solutions*, National Association of Corrosion Engineers., Houston TX (1974).
[120] see also: G. Charlot. *Les réactions chimiques en solution aqueuse et caractérisation des ions*, p. 227, Masson, Paris (1983).
[121] see also: B. Messaoudi, S. Joiret, M. Keddam, H. Takenouti. *Electrochim. Acta* **46**, 2487 (2001).
[122] S. -C. Pang, M. A. Anderson, T. W. Chapman. *J. Electrochem. Soc.* **147**, 444 (2000).
[123] S. C. Pang, B. H. Wee, S. F. Chin. *Int. J. Electrochem.* **2011**, 397685 (2011).
[124] Y. Chen, J. -W. Wang, X. -C. Shi, B. -Z. Chen. *Electrochim. Acta* **109**, 678 (2013).
[125] G. Moses Jacob, I. Zhitomirsky. *Appl. Surf. Sci.* **254**, 6671 (2008).
[126] L. Chen, N. Gu, R. Ding, L. Qi, H. Wang. *J. Solid State Electrochem.* **17**, 2579 (2013).
[127] X. Hong, G. Zhang, Y. Zhu, H. Yang. *Mat. Res. Bull.* **38**, 1695 (2003).
[128] X. Wang, X. Wang, W. Huang, P. J. Sebastian, S. Gamboa. *J. Power Sources* **211**, 140 (2005).
[129] J. Liu, J. Essner, J. Li. *Chem. Mater.* **22**, 5022 (2010).
[130] M. -S. Wu, Z. -S. Guo, J. -J. Jow. *J. Phys. Chem. C* **114**, 21861 (2010).
[131] Q. T. Qu, P. Zhang, B. Wang, Y. H. Chen, S. Tian, Y. P. Wu, R. Holze. *J. Phys. Chem. C* **113**, 14020 (2009).
[132] X. Jin, W. Zhou, S. Zhang, G. Z. Chen. *Small* **3**, 1513 (2007).
[133] H. Wang, C. Peng, J. Zheng, F. Peng, H. Yu. *Mater. Res. Bull.* **48**, 3389 (2013).
[134] R. Zhou, C. Meng, F. Zhu, Q. Li, C. Liu, S. Fa, K. Jiang. *Nanotechnol.* **21**, 345701 (2010).
[135] J. Liu, J. Jiang, C. Cheng, H. Li, J. Zhang, H. Gong, H. J. Fan. *Adv. Mater.* **23**, 2076 (2011).
[136] J. Yan, E. Khoo, A. Sumboja, P. S. Lee. *ACS Nano* **4**, 4247 (2010).
[137] H. Jiang, C. Li, T. Sun, J. Ma. *Nanoscale* **4**, 807 (2012).
[138] B. Ming, J. Li, F. Kang, G. Pang, Y. Zhang, L. Chen, J. Xu, X. Wang. *J. Power Sources* **198**, 428 (2012).
[139] A. J. Roberts, R. C. T. Slade. *Energy Environ. Sci.* **4**, 2813 (2011).
[140] W. Xiao, H. Xia, J. Y. H. Fuh, L. Lu. *J. Power Sources* **193**, 935 (2009).
[141] X. Zhang, X. Sun, H. Zhang, D. Zhang, Y. Ma. *Mater. Chem. Phys.* **137**, 290 (2012).
[142] W. Tang, Y. Y. Hou, X. J. Wang, Y. Bai, Y. S. Zhu, H. Sun, Y. B. Yue, Y. P. Wu, K. Zhu, R. Holze. *J. Power Sources* **197**, 330 (2012).
[143] W. Chen, Z. Fan, L. Gu, X. Baoc, C. Wang. *Chem. Commun.* **46**, 3905 (2010).
[144] J. Chmiola, G. Yushin, Y. Gogotsi, C. Portet, P. Simon, P. L. Taberna. *Science* **313**, 1760 (2006).
[145] J. Chmiola, C. Largeot, P. -L. Taberna, P. Simon, Y. Gogotsi. *Angew. Chem. Int. Ed.* **47**, 3392 (2008).
[146] W. Yang, Z. Gao, J. Wang, B. Wang, Q. Liu, Z. Lia, T. Mann, P. Yang, M. Zhang, L. Liu. *Electrochim. Acta* **69**, 112 (2012).
[147] X. Dong, W. Shen, J. Gu, L. Xiong, Y. Zhu, H. Li, J. Shi. *J. Phys. Chem. B* **110**, 6015 (2006).
[148] M. -W. Xu, W. Jia, S. -J. Bao, Z. Su, B. Dong. *Electrochim. Acta* **55**, 5117 (2010).
[149] R. Liu, S. B. Lee. *J. Am. Chem. Soc.* **130**, 2942 (2008).
[150] S. I. Cho, D. H. Choi, S. -H. Kim, S. B. Lee. *Chem. Mater.* **17**, 4564 (2005) .
[151] D. Zhao, Z. Yang, L. Zhang, X. Feng, Y. Zhang. *Electrochem. Solid-State Lett.* **14**, A93 (2011).
[152] J. Ge, H. -B. Yao, W. Hu, X. -F. Yu, Y. -X. Yan, L. -B. Mao, H. -H. Li, S. -S. Li, S. -H. Yu. *Nano Energy* **2**, 505 (2013).
[153] A. Boisset, L. Athouël, J. Jacquemin, P. Porion, T. Brousse, M. Anouti. *J. Phys. Chem. C* **117**, 7408 (2013).
[154] E. Beaudrouet, A. Le Gal La Salle, D. Guyomard. *Electrochim. Acta* **54**, 1240 (2009).
[155] N. Tang, X. Tian, C. Yang, Z. Pi. *Mater. Res. Bull.* **44**, 2062 (2009).

[156] Y. C. Hsieh, K. -T. Lee, Y. -P. Lin, N. -L. Wu, S. W. Donne. *J. Power Sources* **177**, 660 (2008).
[157] L. Athouël, F. Moser, R, Dugas, O. Crosnier, D. Bélanger, T. Brousse. *J. Phys. Chem. C* **112**, 7270 (2008).
[158] T. Brousse, P. -L. Taberna, O. Crosnier, R. Dugas, P. Guillemet, Y. Scudeller, Y. Zhoud, F. Favier, D. Bélanger, P. Simon. *J. Power Sources* **173**, 633 (2007).
[159] F. X. Wang, S. Y. Xiao, X. W. Gao, Y. S. Zhu, H. P. Zhang, Y. P. Wu, R. Holze. *J. Power Sources* **242**, 560 (2013).
[160] F. X. Wang, S. Y. Xiao, X. W. Gao, Y. S. Zhu, H. P. Zhang, Y. P. Wu, R. Holze. *J. Power Sources* **242**, 560 (2013).
[161] F. X. Wang, S. Y. Xiao, Y. S. Zhu, Z. Chang, C. L. Hu, Y. P. Wu, R. Holze. *J. Power Sources* **246**, 19 (2014).
[162] W. Tang, L. L. Liu, S. Tian, L. Li, L. L. Li, Y. B. Yue, Y. Bai, Y. P. Wu, K. Zhu, R. Holze. *Electrochem. Commun*. **13**, 1159 (2011).
[163] J. Xie, C. -Y. Sun, T. -J. Zhu, G. -S. Cao, X. -B. Zhao, S. -C. Zhang. *J. Solid State Electrochem.* **17**, 2589 (2013).
[164] S. -B. Ma, K. -W. Nam, W. -S. Yoon, X. -Q. Yang, K. -Y. Ahn, K. -J. Oh, K. -B. Kim. *Electrochem. Commun.* **9**, 2807 (2007).
[165] Q. T. Qu, L. Li, S. Tian, W. L. Guo, Y. P. Wu, R. Holze. *J. Power Sources* **195**, 2789 (2010).
[166] L. Mai, H. Li, Y. Zhao, X. Xu, Y. Luo, Z. Zhang, W. Ke, C. Niu, Q. Zhang. *Sci. Rep.* **3**, 1718 (2013); DOI:10.1038/srep01718.
[167] Q. T. Qu, Y. Shi, S. Tian, Y. H. Chen, Y. P. Wu, R. Holze. *J. Power Sources* **194**, 1222 (2009).
[168] T. Tsumura, M. Inagaki. *Solid State Ion.* **104**, 183 (1997).
[169] T. Brezesinski, J. Wang, S. H. Tolbert, B. Dunn. *Nat. Mater.* **9**, 146 (2010).
[170] W. Tang, L. Liu, S. Tian, L. Li, Y. Yue, Y. Wu, K. Zhu. *Chem. Commun.* **47**, 10058 (2011).
[171] L. -Q. Mai, F. Yang, Y. -L. Zhao, X. Xu, L. Xu, Y. -Z. Luo. *Nat. Commun.* **2**, 381 (2011).
[172] L. Zheng, Y. Xu, D. Jin, Y. Xie. *Chem. Asian J.* **6**, 1505 (2011).
[173] Y. Liu, B. Zhang, Y. Yang, Z. Chang, Z. Wen, Y. Wu. *J. Mater. Chem. A* **1**, 13582 (2013).
[174] T. -C. Wen, C. -C. Hu, Y. -J. Li. *J. Electrochem. Soc.* **140**, 2555 (1993).
[175] G. S. Gund, D. P. Dubal, S. B. Jambure, S. S. Shinde, C. D. Lokhande. *J. Mater. Chem. A* **1**, 4793 (2013).
[176] H. Jiang, T. Sun, C. Li, J. Ma. *RSC Advances* **1**, 954 (2011).
[177] J. Y. Lee, K. Liang, K. H. An, Y. H. Lee. *Synthet. Met.* **150**, 153 (2005).
[178] Y. Zheng, M. Zhang, P. Gao. *Mat. Res. Bull.* **42**, 1740 (2007).
[179] P. Lin, Q. She, B. Hong, X. Liu, Y. Shi, Z. Shi. *J. Electrochem. Soc.* **157**, A818 (2010).
[180] R. Zhou, C. Meng, F. Zhu, Q. Li, C. Liu, S. Fa, K. Jiang. *Nanotechnol.* **21**, 345701 (2010).
[181] S. K. Meher, P. Justin, G. R. Rao. *ACS Appl. Mater. Interfaces* **3**, 2063 (2011).
[182] H. Wang, H. Sanchez Casalongue, Y. Liang, H. Dai. *J. Am. Chem. Soc.* **132**, 7472 (2010).
[183] H. Wang, Y. Liang, T. Mirfakhrai, Z. Chen, H. Sanchez Casalongue, H. Dai. *Nano Res*. **4**, 729 (2011).
[184] J. W. Lee, T. Ahn, D. Soundararajan, J. M. Ko, J. -D. Kim. *Chem. Commun.* **47**, 6305 (2011).
[185] S. Yang, X. Wu, C. Chen, H. Dong, W. Hu, X. Wang. *Chem. Commun*. **48**, 2773 (2012).
[186] M. -S. Wu, Y. -P. Lin, C. -H. Lin, J. -T. Lee. *J. Mater. Chem.* **22**, 2442 (2012).
[187] B. Zhao, J. Song, P. Liu, W. Xu, T. Fang, Z. Jiao, H. Zhang, Y. Jiang. *J. Mater. Chem.* **21**, 18792 (2011).
[188] H. -W. Wang, Z. -A. Hu, Y. -Q. Chang, Y. -L. Chen, H. -Y. Wu, Z. -Y. Zhang, Y. -Y. Yang. *J. Mater. Chem.* **21**, 10504 (2011).
[189] H. -C. Chien, W. -Y. Cheng, Y. -H. Wang, S. -Y. Lu. *Adv. Funct. Mater*. **22**, 5038 (2012).
[190] K. R. Prasad, N. Miura. *Electrochem. Commun.* **6**, 849 (2004).
[191] M. Jayalakshmi, N. Venugopal, K. Phani Raja, M. Mohan Rao. *J. Power Sources* **158**, 1538 (2006).
[192] N. -L. Wu. *Mat. Chem. Phys.* **75**, 6 (2002).
[193] C. Wu, F. Feng, Y. Xie. *Chem. Soc. Rev.* **42**, 5157 (2013).
[194] L. -M. Chen, Q. -L. Lai, Y. -J. Hao, Y. Zhao, X. -Y. Ji. *J. Alloys Compd.* **467**, 465, (2009).
[195] Q. T. Qu, L. Li, W. L. Guo, Y. Shi, S. Tian, Y. P. Wu, R. Holze. *Electrochim. Acta* **96**, 8, (2013).
[196] V. S. Reddy Channu, R. Holze, B. Rambabu. *Curr. Appl. Phys.* **13**, 237 (2013).
[197] Z. Chen, Y. Qin, D. Weng, Q. Xiao, Y. Peng, X. Wang, H. Li, F. Wei, Y. Lu. *Adv. Funct. Mater.* **19**, 3420 (2009).
[198] Y. Wang, G. Gao. *Key Eng. Mater.* **336–338**, 2134 (2007).